A strategically designed homogeneous antibody-drug conjugate improves safety and therapeutic index in renal cell carcinoma

Liya Thurakkal[1,2], Krishna Velayutham[1,2], Binayak Sarkar[1,2], Akshaya Kalyan[1,2], Shiladitya Sengupta[1,2,3]*, Tanmoy Saha[1,2]*.

[1]Division of Engineering in Medicine, Department of Medicine, Brigham and Women's Hospital, Harvard Medical School, Boston, MA, USA. [2]Center for Engineered Therapeutics, Department of Medicine, Brigham and Women's Hospital, Harvard Medical School, Boston, MA, USA. [3]Dana Farber Cancer Institute, Boston, MA, USA.

*Corresponding author. Email: ssengupta2@bwh.harvard.edu (S.S.); tsaha2@bwh.harvard.edu (T.S.)

ABSTRACT

Renal cell carcinoma (RCC) is one of the leading causes of kidney cancer-related mortalities worldwide. Though the treatment method of RCC has advanced from nephrectomy to targeted therapy and immunotherapy, most patients suffer from therapeutic resistance, metastasis, and relapse. In recent days, antibody drug conjugates (ADCs) have emerged as a promising treatment modality by delivering cytotoxic payloads specifically to the cancer cells. However, previous efforts related to ADC have failed in the clinic because of severe toxicity. Here, we introduced a homogenous ADC (LT-025), which can target the kidney injury molecule (KIM) -1 receptor on RCC cells. We adopted the enzymatic conjugation involving microbial transglutaminase (MTGase) to attach the cytotoxic drug DM1 to the Fc region of the KIM-1 antibody. We demonstrated a site-specific conjugation of the drug-linker with a specific drug-to-antibody ratio (DAR) of 2. The ADC exhibited prolonged stability and superior antigen-binding capability, characterized using various bioanalytical methods. We proved that cellular internalization and cytotoxicity are dependent on the KIM-1 expression on RCC. The LT-025 displayed superior cytotoxicity to the metastatic RCC cells, then standard RCC treatment by sunitinib. The combination therapy of LT-025 and sunitinib showed increased therapeutic efficacy in vitro in RCC as well as in sunitinib-resistant RCC models. The LT-025 exhibited a safe and effective treatment in the syngeneic RCC mouse model. The combination therapy also showed an increased tumor growth inhibition in preclinical mouse model studies. A carefully designed KIM-1 targeting ADC can emerge as an effective treatment method for metastatic RCC.

INTRODUCTION

Kidney cancer is one of the ten most prevalent cancers worldwide, resulting in more than 430,000 cases each year.[1] Renal Cell Carcinoma (RCC) comprises nearly 90% of all kidney cancer types.[2] The majority of the RCC patients are treated with surgery, known as nephrectomy.[3,4] Though nephrectomy has shown adequate outcomes in patients with localized diseases, the overall outcome is poor because of relapse and metastasis. In fact, more than 35% of the RCC patients experienced metastasis to distant organs and exhibited a 5-year survival of only 10-15%.[5] As an alternative approach, targeted therapy, such as sunitinib, sorafenib, everolimus, and axitinib, was tried but often encounters drawbacks because of insufficient efficacy or adaptive treatment resistance.[6-8] Additionally, several immunotherapies have shown considerable progress as a second line of treatment or adjuvant therapy; however responsive to only a fraction of patients.[9-11] Chemotherapy has never appeared to be an effective first line of therapy for RCC because of inadequate therapeutic response and toxic effects on normal kidney cells.[12,13] However, the toxicity can be significantly reduced by selectively delivering the chemotherapy agent to the cancer cells, thereby offering a safe and effective treatment outcome.

Over the last decade, the use of antibody-drug conjugates (ADCs) has gained attention because of their capability of delivering payloads specifically to cancer cells.[14] Antibodies against cancer cell-specific antigens are linked with a cytotoxic payload via a linker to achieve ADCs. The antibodies were rationally selected based on the biomarkers expressed on the cancer cells. Currently, several ADCs have shown promising outcomes in the clinic.[15,16] However, off-target toxicity, premature release of payload, and the heterogeneous conjugation of the antibody and the drug are a few reasons for the failure of many ADCs in clinical trials.[17] In fact, an ADC against RCC, known as CDX-014, has been developed in the past targeting kidney injury molecule-1 (KIM-1), but failed during clinical evaluation.[18,19] KIM-1 is a glycoprotein, also known as T-cell immunoglobulin and mucin domain–containing protein 1 (TIM-1), absent in normal kidney cells but upregulated in cases of kidney injury, including kidney cancer.[20-23] The previous CDX-014 was constructed by combining the KIM-1 antibody and MMAE as a cytotoxic payload.[24] Despite showing promising preliminary tumor regression, the clinical trial was aborted because of the toxic outcome to the patients, including grade 3 toxicity and treatment-related death.[25] Where many factors could be responsible for the toxicity, the premature release of the payload and off-target delivery are critical drawbacks of the ADC's design, resulting in a toxic outcome.

The linker and the conjugation chemistry for attaching the drug to the antibody play a critical role in the stability and the efficiency of the ADC. The peripheral blood testing of patients treated with CDX-014 revealed free MMAE in the blood samples, indicating possible premature release of the payload. Given the high cytotoxic potency of MMAE, the early release of the drug from the antibody may have contributed to the observed toxicity. The CDX-014 design used a cleavable linker with a heterogeneous cysteine conjugation. The heterogeneous ADC experience limitations related to reduced stability, off-target toxicity, and an inconsistent therapeutic window.[26-29] Moreover, the use of a cleavable linker poses the risk of linker instability, resulting in premature release of the drug. This challenge can be effectively addressed by adopting a strategic design of the ADC. This approach should prioritize the optimal selection of conjugation and linker chemistry to achieve advantageous results.

Here, we developed a homogenous KIM-1 ADC (LT-025) with DM1 as the cytotoxic payload. To design a homogenous KIM-1 ADC, we adopted a site-specific enzymatic conjugation of the drug-linker with the KIM-1 antibody. We demonstrated the microbial transglutaminase (MTGase) mediated transamidation reaction at the Fc region of the antibody with an amine-functionalized DM1-linker. According to our hypothesis, a homogeneous ADC could impart advantages related to stability and specificity, resulting in reduced off-target toxicity. The homogenous ADC is prepared to yield a uniform product with a specific drug-to-antibody ratio (DAR). We performed a detailed biophysical characterization of the ADC, including antigen-binding capability, DAR, and stability, signifying the potential of the ADC. The detailed in vitro and in vivo studies represent the therapeutic outcome of the LT-025. We also demonstrated whether the ADC could enhance the treatment response in combination with standard sunitinib treatment in metastatic RCC and sunitinib-resistant RCC models.

RESULT

KIM-1 expression in renal cell carcinoma tissue and adjacent normal tissue

At first, we confirmed the KIM-1 overexpression in RCC tissues over other normal adjacent tissues. According to The Cancer Genome Atlas (TCGA) database, the median expression of KIM-1 transcript per million (TPM) in kidney cancer and normal kidney cells is 25.73 and 3.6, respectively (**Supplementary Fig.1a**). The Gene Expression Profiling Interactive Analysis (GEPIA) analysis of the KIM-1 revealed its expression exclusively in the kidney and expressively upregulated in the case of kidney cancer (**Fig.1a, supplementary Fig.1**). Next, we performed immunohistochemistry to investigate the expression of the KIM-1 in RCC patient-derived tissue samples in tumor tissue with the adjacent normal kidney tissue of the matched patient. We used a tissue microarray

of 16 RCC patients randomized based on age (26 to 79 years), sex, and cancer stage (I to III) containing tumor and normal adjacent tissue (NAT) specimens. Immunostaining of the tissue samples revealed high KIM-1 expression in RCC specimens (**Fig.1b**). We have quantified the KIM-1 intensity and normalized it with the tissue density for each cancer and normal adjacent tissue (NAT). We found a significantly higher KIM-1 expression in cancer tissue than its matched NAT in 11 out of 16 patients (**Fig.1c**). This observation validates the known 70% KIM-1 positive RCC patients' data in the literature.[20,21,23,30-32] The significantly higher KIM-1 expression in cancer tissue in the majority of the RCC patients allowed it to become a promising target for the antibody-drug conjugate.

LT-025 (KIM-1 ADC) development and biophysical characterization

We adopted a homogenous ADC design by site-specific conjugation of the drug-linker with the KIM-1 antibody. We selected an enzymatic site-specific conjugation of the drug-linker at the Fc region of the antibody to avoid any interference with the antigen-binding site. In this method, we can start with a native antibody and conjugate any amine-functionalized drug-linker. We used Mertansine (DM1), a potent microtubule inhibitor, as the payload. DM1 is a popular payload for ADC design because of its excellent cytotoxicity.[33,34] At first, the drug-linker, DM1-PEG_9-NH_2, was synthesized by conjugating DM1 with a PEG_9-NH_2 linker using thiol maleimide chemistry (**supplementary Fig.2a**). We characterized the DM1-linker with ^{1}H Nuclear Magnetic Resonance (NMR), ^{13}C NMR, and mass spectrometry (**supplementary Fig.2b,c, and 3b**). The purity of the linker was determined using liquid chromatography (LC) before proceeding with the antibody conjugation (**supplementary Fig.3a**).

We used Microbial Transglutaminase-mediated (MTGase) conjugation, which exclusively conjugates the drug-linker at the Q295 position of the Fc region of the IgG1 antibody.[35] However, in the native form of the antibody, Q295 is not accessible to the MTGase because of the presence of N-glycans at the N297 location. So, at first, we performed deglycosylation of the native antibody using the standard PNGase-F method, which selectively removed the polysaccharide unit from the N297 position (**Fig.2a**).[36,37] We monitored the deglycosylation reaction using hydrophobic interaction chromatography (HIC) and confirmed with mass spectrometry (**Fig.2b,c**). The HIC chromatogram showed an increase in retention time, due to the change in the hydrophobicity of the antibody (**Fig.2b**) upon removal of N-glycan. The observed loss of 1445 Da mass in ESI-MS of heavy chain, confirmed the successful deglycosylation from heavy chain region with no change in the light chain mass (**Fig.2c**). Next, the DM1-PEG_9-NH_2 linker was attached to the antibody in the presence of MTGase, which catalyzes an acyl transfer reaction between the γ-carboxyamide group of a glutamine (Q295) on the antibody with a primary amine. We have optimized the MTGase conjugation of the drug-linker with the deglycosylated antibody to yield a homogeneous ADC with maximum yield (**supplementary Fig.4**). The single peak at the HIC chromatogram with a higher retention time than the deglycosylated antibody stands for the exclusive formation of the desired ADC. An increase of 1327 Da mass of the heavy chain confirms the conjugation of a single drug-linker per heavy chain (**Fig.1b,c**). We observed increased yield of the ADC while using the Enhanced Microbial Transglutaminase (eMTGase) over the classical MTGase (Activa TI Transglutaminase). However, using eMTGase often results in a hyper-conjugated product with more than one drug conjugation in each heavy chain, as indicated in some of the previous reports.[38] We performed detailed optimization of reaction conditions in order to achieve a homogeneous ADC. **Supplementary Fig.4a,b** represents the optimized reaction condition with a single ADC product. We found that the deglycosylation step is essential to achieve a homogeneous ADC with one conjugation per heavy chain of the antibody. To verify that we attempted the transamidation reaction with the native antibody without the deglycosylation step. This reaction resulted in most of the unreacted antibody with one minor product, which did not match our desired ADC (**Fig.2d**).

We calculated the drug-to-antibody ratio (DAR) using UV-visible spectroscopy and confirmed via ESI-MS. At first, we calculated the molar extinction coefficient of the DM1-linker and antibody at 254 and 280 nm (**supplementary Fig.5**). The absorption of the ADC was checked at 254 and 280 nm, and the DAR was calculated according to equations 1, 2, and 3 as mentioned in previously reported literature[39,40]. We observed a DAR of 2 for LT-025. This was also validated from the HIC and ESI-MS data, where one drug-linker is conjugated with each heavy chain of the antibody. This supports our hypothesis on the use of the MTGase-mediated bioconjugation to produce homogenous ADC. The LT-025 has shown stability for more than 15 days in mouse plasma. To study that, we incubated the LT-025 in mouse plasma at 4 ^{o}C, and room temperature, and the stability was investigated using the HIC chromatography. The area of the peak corresponds to the ADC in the HIC-chromatogram was plotted in **Fig.2e**. The data show no significant change in the stability in either of the conditions for 15 days.

The conjugation of the drug-linker with the antibody may impact its binding to the KIM-1 protein in cancer cells. We used an enzyme-linked immunosorbent assay (ELISA) to investigate the antigen recognition capability of the LT-025 and compared it with the native KIM-1 antibody. We used a KIM-1 protein-coated ELISA plate to investigate the binding with the KIM-1 antibody and LT-025. We confirmed that the ADC can bind with the antigen in a concentration-dependent manner (**Fig.3a**). The antigen-binding of LT-025 obtained by the ELISA matched the native antibody, signifying no loss of antigen-binding property during the conjugation. Additionally, we used a competitive binding assay where the antigen binding of ADC was compared with a 1:1 mixture of native antibody and ADC. We observed a 50% reduction in the ADC binding with the antigen, as the remaining 50% has been occupied by the native antibody (**Fig.3b**). This confirms the comparable antigen-binding capability of the ADC and the native antibody.

Next, in order to get quantitative insight into the antigen-binding ability of ADC, we used biolayer interferometry (BLI) analysis. The ADC showed a dose-dependent association and dissociation kinetics with the KIM-1 antigen-coated BLI sensor chip (**Fig.3c**). The LT-025 showed similar association and dissociation kinetics as the native KIM-1 antibody. The calculated dissociation constant of the LT025 and the native antibody are $K_D = 0.597 \pm 0.008$ nM, and $K_D = 0.33 \pm 0.008$ nM, respectively (**Fig.3d**). This suggests that the deglycosylation followed by homogenous conjugation has no significant effect on antigen recognition as compared to the native antibody.

Antibody-fluorophore conjugate for evaluating reproducible conjugation and cellular internalization:

We prepared an antibody-fluorophore conjugate (AFC) to verify the robustness of the conjugation and to investigate the cellular internalization and localization. A Cy5 fluorophore (**supplementary Fig.6a**) linker was used because of its biocompatibility and strong fluorescence signal. This enables easy estimation of cellular internalization and localization. The NH_2-functionalized Cy5-linker was conjugated with the KIM-1 antibody to produce AFC following the similar enzymatic method as mentioned for the ADC (**Fig.4a**). The conjugation reaction of the Cy5-linker was further confirmed by the HIC chromatography (**supplementary Fig.6b**). The peak at 280 nm and 649 nm HIC chromatogram signifies the specific antibody and Cy5 fluorophore conjugation, resulting in exclusively desired homogenous AFC. We confirmed the conjugation specificity in the heavy chain by using SDS-polyacrylamide gel electrophoresis (SDS–PAGE). A denaturing buffer was used to separate the heavy and light chains of the antibody. The presence of the Cy5 fluorescence was observed exclusively at the 50 kDa, corresponding to the selective conjugation in the heavy chain of the antibody (**Fig.4b**). No fluorescence was observed in the light chain of the antibody.

ADCs are designed to bind with cell surface receptors, followed by receptor internalization by endocytosis (**Fig.4c**). We used a metastatic renal cell carcinoma cell line, Renca, having significant KIM-1 expression (**supplementary Fig.8**). We observed a rapid cellular internalization of AFC in Renca cells using flow cytometry

(**Fig.4d**). The histogram represents the increase in the mean fluorescence intensity corresponding to increased cell surface receptor recognition and internalization of AFC with time. But the flow cytometry data cannot differentiate between the receptor binding on the surface and internalization. Thus, we performed time-dependent confocal microscopy to investigate the cellular internalization and localization. **Fig.4e** shows a considerable amount of cellular internalization of the AFC in Renca cells within 30 minutes and an increased cellular internalization at 4 h. Moreover, we used a lysotracker red dye to evaluate the lysosomal localization of the AFC. We observed localization of the AFC in the lysosomal compartments. Quantification of the colocalization between AFC and lysotracker signal revealed increased colocalization at 4 h compared to 30 minutes (**supplementary Fig.7**). This is in accordance with the hypothesis that AFC and ADC first bind with the cell surface receptor, followed by the receptor internalization and localization to the lysosomal compartment.[41]

Next, to confirm that the cellular internalization of the AFC is dependent on the KIM-1 expression on the kidney cancer cell, we generated a KIM-1 overexpressing Renca cell line ($Renca^{KIM\text{-}1++}$) by lentiviral transduction. The overexpression of KIM-1 in $Renca^{KIM\text{-}1++}$ was characterized using Western blot and flow cytometry analysis. The $Renca^{KIM\text{-}1++}$ showed 3 times more KIM-1 expression than wild-type Renca cells (**supplementary Fig.8a,b**). Flow cytometric analysis revealed an elevated cellular internalization of AFC in $Renca^{KIM\text{-}1++}$ cells compared to Renca cells (**supplementary Fig.8c**). The mean fluorescence intensity (MFI) of AFC showed significantly higher cellular internalization of AFC in the case of $Renca^{KIM\text{-}1++}$ than the wild-type Renca, suggesting the antigen-dependent internalization (**supplementary Fig.8d**).

In vitro cytotoxicity

Cellular internalization directly correlates with the cytotoxicity of the ADC. We evaluated the cytotoxicity of ADC in Renca cells using MTT cell viability assay. We observed strong cytotoxicity in nanomolar concentrations of the LT-025 with a low IC_{50} of 88.67 nM (**Fig.5a**). To investigate the KIM-1 dependency on the cytotoxic effects, we next used the $Renca^{KIM\text{-}1++}$ cell line. A notably higher cytotoxicity was observed in $Renca^{KIM\text{-}1++}$ with a lower IC_{50} of 11.78 nM (**Fig.5b**). Next, we compared the cytotoxicity of LT-025 with a KIM-1 MMAE ADC, which matches the previously reported heterogeneous ADC design.[24,25] The KIM-1 MMAE ADC used a maleimide-cysteine coupling to generate a heterogeneous ADC. We found a significantly higher cytotoxicity with our homogenous LT-025 than previously used KIM-1 MMAE ADC (**Fig.5c**).

Next, we provided mechanistic insight into the cytotoxicity of the LT-025. The payload used in LT-025, DM1, is a known microtubule inhibitor and imposes mitotic arrest followed by cancer cell killing. It prevents microtubule dynamics by binding to the tubulin and converts them to random tubulin aggregates or monomer form[42]. We encountered a substantial reduction of microtubule formation in the Renca cells by ADC using high-resolution confocal microscopy (**Fig.5d,e**). The untreated control Renca cells showed microtubules as a thread-like structure, but the microtubules appeared as an aggregated form in the LT-025 treated cells (**Fig.5d, supplementary Fig.9**). Moreover, the quantification of such confocal images attributed a significant reduction in the tubulin intensity and the overall cell volume for LT-025 treated cells in comparison to the control (**Fig.5e,f**). The LT-025 also increased the E-cadherin amount in the Renca cells when applied at low concentration, signifying the suppression of epithelial to mesenchymal transition (EMT) and reduction in metastatic potential (**supplementary Fig.10**).

Sunitinib, a tyrosine kinase inhibitor, is used as a standard first line of treatment for metastatic RCC patients.[43-45] However, often results in insufficient therapeutic efficacy because of the adaptive drug resistance. We studied the effect of LT-025 in combination with sunitinib on cell viability in Renca. We used a mixture of sunitinib (12.5 μM) and LT-025 (100 nM) and evaluated the apoptosis induction by flow cytometry analysis. **Fig.5g** shows a significantly higher apoptosis induction in the LT-025+sunitinib treated cells compared to the untreated control

and monotherapy. Next, we have generated a sunitinib-resistant Renca cell line by increasing the concentration of sunitinib according to the reported procedure.[46] We investigated the effect of LT-025 on sunitinib-resistant cells, alone and in combination with sunitinib. The combination of LT-025+sunitinib showed a significantly enhanced apoptosis induction compared to monotherapies in sunitinib-resistant Renca cells (**Fig.5h**). Hence, the combination of LT-025+sunitinib has the potential to offer enhanced therapeutic outcomes in RCC.

In vivo efficacy

Treatment-related toxicity is one of the major concerns for KIM-1 targeting ADC, as one such ADC has failed in the clinic.[25] As a first step, we performed a detailed toxicity evaluation by a dose escalation study in immunocompetent balb/c mice. We injected LT-025 via the tail vein at a 3-4 day interval with an increasing dose of 0.83 to 3.33 mg/kg. No significant body weight loss or visible signs of toxicity were found (**Fig.6a**). We sacrificed 5 mice after the 1.67 mg/kg dose and the rest after the 3.33 mg/kg dose to evaluate any toxicity related to the liver and kidney. We performed detailed biochemistry analysis for liver, kidney enzymes, and the critical components in the serum. No abnormal change in blood alkaline phosphatase (ALP), aspartate aminotransferase (AST), alanine aminotransferase (ALT), Creatine kinase, total protein, globulin, albumin, bilirubin, and blood urea nitrogen (BUN) was observed in either of the doses (**Fig.6b, supplementary Fig.11**), signifying safe treatment of the LT-025 within the dose range of 0.83 - 3.33 mg/kg.

Next, we used the syngeneic Renca tumor model in balb/c mice to evaluate the tumor growth inhibition by LT-025 as a monotherapy and in combination with sunitinib. A subcutaneous tumor was implanted in the right flank of the male balb/c mice. The mice were monitored for their body weight and tumor growth. We randomized the mice into 4 groups once the tumor became 50-75 mm^3. Mice were dosed with 1.67 mg/kg of LT-025 on days 8, 12, 17, and 21 using intravenous injection. Sunitinib (20 mg/kg) was given orally on days 7, 11, 16, and 20 (**Fig.6c**). The LT-025 treated group showed reduced tumor growth than control mice (**Fig.6d**). Moreover, the combination of LT-025 and sunitinib showed increased therapeutic efficacy than monotherapies. This represents that the combination of the LT-025 and sunitinib can show an increased therapeutic outcome by overcoming the adaptive drug resistance. We did not observe any significant treatment-related toxicity in the mice.

DISCUSSION

Kidney cancer patients generally undergo nephrectomy as a first line of treatment. The therapeutic outcome for chemotherapy is less due to insufficient efficacy and toxicity to the normal kidney cells. Here, we introduce a KIM-1 targeting antibody drug conjugate, LT-025, which selectively delivers the chemotherapy drug to the kidney cancer cells. According to the literature reports[20-23] and our observation, KIM-1 is overexpressed in kidney cancer than in neighboring normal kidney tissue. We found, using patient biopsy analysis, that the majority (70%) of the patients have significantly higher KIM-1 expression in cancer tissue than in the adjacent normal tissue. This eliminates the possibility of the off-target effects for the ADC. Thus, it makes KIM-1 a promising target for the ADC design. However, efforts have failed previously for the approval of KIM-1 targeting ADC. The major concern of the previously used ADC was the treatment-related toxicity generated from two major reasons: (i) off-target engagement of the ADC, (ii) premature release of the payload from the antibody.

Several ADCs have failed in clinical trials because of insufficient therapeutic efficacy and treatment-related toxicity. In fact, the previously tried KIM-1 targeting ADC also failed because of the grade 3 toxicity among the patients and treatment-related death.[25] Heterogeneous ADC leading to inconsistent DAR and premature release of the drug may cause toxic effects. Here, we adopted a site-specific bioconjugation approach to achieve a

homogenous ADC. We used an enzymatic transamidation reaction in specific glutamine residues in the Fc region of the native antibody. The conjugation followed a two-step process: (i) deglycosylation of the antibody using PNGaseF enzyme, (ii) MTGase-based conjugation of the NH_2-functionalized drug-linker with Q295 of the heavy chain of the KIM-1 antibody, having IgG1 subtype. The regioselectivity of the conjugation on the Q295 over other glutamine residues is likely governed by (i) the availability of the glutamine on the surface for the enzyme to bind and (ii) the flexibility of the region known as the B-factor.[47] However, in the native IgG1 antibody, the Q295 position is sterically hindered because of the presence of the glycan at N297. PNGase-F based method of deglycosylation selectively removes the polysaccharide unit from the N297 position.[36,37] The removal of the Fc glycan not only offers increased accessibility of the Q295, also increases the flexibility of the region.[48,49] Fontana et al. have shown the relation of the flexibility of the polypeptide chain with the selectivity of the MTGase reaction.[47]

We selected the MTGase-mediated site-specific glutamine addition reaction over other homogenous conjugation strategies because of (i) the use of the natural Fc region of the antibody, (ii) the specificity of the reaction. This allows us to use such chemistry for other antibodies without proceeding with any protein engineering. We used a commercially available KIM-1 antibody, rat IgG1 format. This strategy helps in the future to use any IgG1 antibody for designing other ADCs. We obtained a DAR of 2 in LT-025, i.e, one drug conjugation per heavy chain. This conjugation at the heavy chain is also verified in the case of AFC. The HIC chromatogram showed a single major product, signifying that the DAR=2 stands for the overall DAR of the ADC. This eliminates the requirement of calculating the average DAR from multiple peaks of the HIC chromatogram, a common method followed in the case of heterogeneous ADC.[50]

Apart from conjugation, the stability of the ADC in plasma is also attributed to the safe and effective treatment. We used a PEG-based non-cleavable linker to conjugate the drug to the antibody. Non-cleavable linker has the advantage of lower premature release over the cleavable linker, which could possibly reduce the off-target toxicity.[51] At the same time, it should also be ensured that the drug DM1, along with the linker, is potent enough to exert its cytotoxic action. Trastuzumab DM1 (T-DM1, Kadcyla), a clinically approved ADC, is constructed with a non-cleavable linker and has shown successful payload delivery to the tumor cells.[52] The non-cleavable linker design used in LT-025 is advantageous in reducing the distribution of payload to neighboring cells, known as the bystander effect.[53] Moreover, in the event of unexpected premature cleavage of the drug linker from the antibody, the NH_2 functionalized linker will be restricted from permeabilizing through the membrane because of its cationic form at the physiological pH.[54] This strategy helps in limiting the toxic side effects in the adjacent normal tissue.

Our homogenous ADC design in LT-025 did not interfere with the antigen-binding capacity. We performed antigen recognition and binding experiments using ELISA and BLI. The LT-025 showed identical antigen binding as the KIM-1 antibody. The LT-025 also showed successful internalization in the cell, which is dependent on the KIM-1 expression on the kidney cancer cells. LT-025 showed cytotoxicity in the nanomolar range, signifying effective cancer cell killing. Moreover, treatment of LT-025 to Renca cells has increased its E-Cadherin expression, correlating with reduced metastatic phenotype. LT-025 also showed significantly higher cytotoxicity than the previously used KIM-1-MMAE ADC. This is because the previous KIM-1-MMAE ADC has followed a heterogeneous conjugation approach, which may have compromised the antigen-binding capability. Moreover, the higher chance of aggregation due to stochastic conjugation could lead to a limited cytotoxic effect of KIM-1-MMAE ADC in the cancer cells.

We presented the preclinical studies related to a potential treatment method for kidney cancer patients. The LT-025 can be used as a primary treatment method or in combination with other standard therapy. Sunitinib, a kinase

inhibitor, is a standard treatment method in the clinic for early-stage RCC.[55,56] However, it does not respond to the advanced RCC and is likely to relapse in 6-15 months.[57,58] More than 60% of sunitinib-treated patients develop drug resistance.[59-62] Moreover, the combination of sunitinib with other kinase inhibitors did not show a promising outcome.[63,64] We showed a synergistic outcome of sequential treatment of a combination of sunitinib and LT-025. We used a low dose of ADC and sunitinib to avoid any toxic effect, where the monotherapies showed a significant tumor growth reduction. Interestingly, the combination therapy showed synergistic tumor growth reduction in the metastatic RCC tumor model in a syngeneic balb/c mouse. This report highlights the preclinical study for a potential combination therapy approach for advanced RCC. However, we acknowledge the possible obstacle of administering an ADC and a pharmacological drug because of their different pharmacokinetics and biodistribution, which may appear as a limitation in terms of clinical translation. So, a dual drug ADC having sunitinib and DM1 may be beneficial in this regard. Research in the line of dual drug conjugated homogenous ADC is in progress.

In conclusion, our study indicates that a KIM-1 targeting ADC (LT-025) can offer a promising therapeutic outcome for metastatic RCC tumors. We have meticulously designed a homogenous ADC that exhibits remarkable stability and antigen-binding capability. Unlike the previously reported KIM-1 ADC, the LT-025 offered a safe treatment modality because of (i) homogenous conjugation, (ii) a stable, non-cleavable linker, and (iii) a strategic design to reduce bystander effect. The preclinical evaluation using a syngeneic RCC tumor model in balb/c mice demonstrated the antitumor efficacy and safety of the LT-025. We provided pre-clinical evidence of increased therapeutic outcome by combining the potency of LT-025 with the existing drug sunitinib. The favorable outcome in tumor reduction with minimal toxicity enhances the potential of LT-025 for further advancement in the future.

MATERIALS AND METHODS

Synthesis of the drug-linker

In a clean and dry round-bottom flask, Mal-amido-PEG_9-NH_2 (Broadpharm, 0.020 mmol) was mixed with acetonitrile under an inert atmosphere. N, N-Diisopropylethylamine (DIPEA, 0.1 mmol) was added, followed by the addition of DM1 (MedChemExpress, 0.024 mmol). The mixture was stirred at room temperature for 3 hours. After the reaction, acetonitrile was evaporated in vacuo, and the residue was extracted using ethyl acetate and water. The organic layer was collected and dried over Na_2SO_4. The residue was washed with 20% ethyl acetate and hexane to remove the excess unreacted DM1. The expected compound was collected, dried under vacuum, and characterized by NMR and mass spectrometry. The product was characterized by ^{1}H NMR and ^{13}C NMR using Bruker Avance-III HD Nanobay spectrometer, 400.09 MHz. ^{1}H-NMR spectrum (400 MHz, $CDCl_3$) of DM1 linker. δ (ppm) 0.81 (s, 3H), 1.437 (s, 3H), 1.47 (s, 3H), 1.57 (t, 2H), 1.60 (t, 2H), 1.66 (s, 3H), 2.11 (s, 3H), 2.22 (d, 1H), 2.59 (q, 1H), 2.64 (d, 2H), 2.87 (s, 3H), 2.9 (t, 2H), 3.04 (d, 3H), 3.10 (t, 2H), 3.22 (s, 3H), 3.38 (s, 3H), 3.43 (t, 2H), 3.52 (t, 1H) 3.69 (m, 32H), 3.81 (q, 2H), 3.92 (t, 1H), 4.01 (s, 3H), 4.30 (t, 1H), 4.79 (d, 1H), 5.39 (q, 1H), 5.61 (t, 1H), 6.3 (d, 1H), 6.45 (t, 1H), 6.65 (s, 1H), 6.84 (s, 1H). ^{13}C NMR (101 MHz, $CDCl_3$) of DM1 linker δ (ppm) 176.64, 174.54, 170.82, 170.45, 168.86, 161.84, 156.07, 152.35, 142.23, 141.21, 139.34, 133.37, 127.65, 125.34, 122.23, 118.82, 113.27, 88.65, 80.97, 78.31, 74.23, 70.57, 70.01, 69.84, 60.06, 56.69, 53.97, 52.47, 46.73, 42.05, 40.25, 39.94, 38.99, 37.81, 35.95, 35.60, 34.31, 33.46, 32.54, 30.82, 26.88, 19.91, 18.70, 17.58, 15.64, 14.70, 13.50, 12.30, 11.92. The liquid chromatography and mass spectrometry (LC-MS) of the product was carried out in Agilent 6125B mass spectrometer attached to an Agilent 1260 Infinity LC. Calculated mass for $[M+H]^+$: 1345.6 Da, observed mass: 1345.6 Da. A gradient method of 100% water to 100% acetonitrile in the presence of +0.1% formic acid was used for HPLC using a C18 column.

Synthesis of ADC (LT-025)

Deglycosylation: KIM-1 antibody (anti-mouse, Rat IgG1, BioXcell, 2 mg/mL in PBS) was taken and added 2 µL of PNGase F (New England Biolabs, 1000 units). Incubated at 37 ºC for 20 h. The solution was filtered through 50 kDa Amicon filters three times using PBS and diluted to a 10 mg/mL concentration.

Antibody-Linker Conjugation: Deglycosylated KIM-1 antibody (5 mg/mL in 1:2 PBS and HEPES buffer) was incubated with the linker (18.5 µl, 50 eq, 20 mg/mL in DMSO) and enhanced transglutaminase enzyme (Sigma Aldrich, 22.7 µl, 2.5 eq) at 37 ºC for 20 h. The antibody-drug conjugate formed was purified using 50 kDa Amicon filters by washing with PBS five times. The product was purified from the trace amount of remaining enzyme using protein A agarose beads (Santacruz, 200 µL). After the conjugation reaction, protein A agarose solution was added and incubated at 4 ºC for 1 h. The beads were washed with PBS three times in a mini spin column (QIAmp), and then added 0.1 M glycine, pH: 3.2 solution to elute the ADC. This was further subjected to buffer exchange with PBS, pH 7.4, using Amicon filters, and the product LT-025 was stored at 4 ºC. The final concentration of the ADC was measured using a Thermoscientific NanoDrop One.

Synthesis of Cy5-AFC

The deglycosylated KIM-1 antibody (5 mg/mL) was diluted in 1:2 PBS and HEPES buffer and mixed with Cy5 linker [N-(m-PEG4)-N'(amino-PEG3)-Cy5, Broadpharm, BP-23008, 40 eq., 8.7 µL from 20 mg/mL stock solution in water] and enhanced transglutaminase enzyme (22.7 µL). The mixture was incubated at 37 ºC for 20 h in the dark. The antibody-fluorophore conjugate (AFC) formed was purified using 50 kDa Amicon filters by washing with PBS five times.

Characterization of ADC using Hydrophobic Interaction Column Chromatography

The conjugation efficiency was monitored using hydrophobic interaction column (HIC) chromatography using Agilent 1200 HPLC system connected with a Butyl-NPR column (3.5 cm x 4.6 mm, 2.5 µm particle size). Mobile phase A: 25 mM phosphate buffer pH 7 containing 1.5 M ammonium sulfate, and B: 25 mM phosphate buffer pH 7 containing 20% isopropanol, were run at a gradient from 0% to 100% B at the flow rate of 0.5 mL/min.

Electron Spray Ionization-Mass Spectrometry (ESI-MS)

The antibody and ADC samples were reduced with dithiothreitol (DTT) to separate into heavy and light chains. The solution was then washed and desalted using 3000 MWCO Millipore Amicon filters. 5 µg of sample was directly injected (bypassing column) into the Agilent 1100 High-Performance Liquid Chromatography (HPLC) connected with a Bruker Maxis Impact LC-q-TOF Mass Spectrometer in the presence of the solvents acetonitrile-water with 0.1% formic acid. We have recorded a mass range from 300 Da to 3000 Da. And the signals were deconvoluted to obtain the total mass of the reduced antibody.

Immunohistochemistry and image analysis

Tissue microarrays (TMA) for RCC patients' biopsies (KD321a) were obtained from TissueArray.com. The TMA has cancer and matched adjacent normal kidney tissue from patients randomized based on age, sex, and stage of

the cancer. The FFPE tissue sections were deparaffinized by dipping into xylene and rehydrated by the gradient of the ethanol-water mixture. The antigen retrieval of the tissue specimen was performed using citrate and Tris buffer at 95 °C. The blocking step was done by 5% bovine serum albumin, and 2% goat serum. Antibody staining was performed by specific primary antibody anti-human-KIM-1 (Cell Signalling Technology, Cat. No. 14971, 1:100 dilution), followed by secondary antibodies (anti-rabbit AF488, Thermo Fisher Scientific, Cat. No. A11008, 1:1000 dilution). Images were acquired in a TissueFAXS Plus slide scanner (TissueGnostics USA) equipped with a Hamamatsu Orca Flash 4.0 V2 cooled digital CMOS camera and Zeiss 20x EC Plan-NEOFLUAR 0.5NA air objective. Each image of the tissue specimens is composed of 16 individual image view fields. The quantification of KIM-1 was carried out by measuring the mean pixel intensity using Image*J* software and normalizing with the mean pixel intensity of DAPI.

Cell culture

Murine renal cell carcinoma, Renca (ATCC, CRL-2947), was cultured in RPMI-1640 (ATCC) supplemented with 10% v/v heat-inactivated fetal bovine serum (FBS) (Thermo Fisher Scientific) and 1% v/v Penicillin-Streptomycin (Thermo Fisher Scientific). Cells were cultured, maintained in sterile conditions, and housed in a water-jacketed CO_2 incubator with an atmosphere at 37 °C and 5% CO_2. Cells were routinely tested and mycoplasma-free.

Flow cytometry for cellular internalization

Renca cells were seeded in a culture-treated 24-well plate (100k cells per well) and incubated at 37 ºC under 5% CO_2 for 24 h. The AFC sample (50 µg/mL) was added to the fresh media after a wash with DPBS and incubated under the same conditions for different time points, such as 1 h, 4 h, 12 h, and 24 h. After the time, the cells were washed with DPBS two times and collected after trypsinization. The collected cells were resuspended in 300 µL of cell staining buffer to run the flow cytometry. An Agilent Novocyte flow cytometer was used, and the data were analyzed using FlowJo.

Immunostaining, fluorescence, and confocal microscopy

Renca cells were seeded on sterile 12 mm coverslips in a 24-well plate (100k cells per well) and incubated at 37 ºC under 5% CO_2 for 16 h. The AFC sample (50 µg/mL) was added to the fresh media after a wash with DPBS and incubated under the same conditions for different time-points, such as 0.5 h, 4 h. The cells were washed, and 500 nM of Lysotracker dye (red, Invitrogen) was added and incubated for 30 min. Later, the cells were fixed with 4% paraformaldehyde (Electron Microscopy Sciences), followed by staining with Phalloidin 488 (green, Invitrogen, 1: 400) at an incubation time of 1 h. The nucleus staining was carried out using Hoechst (blue, Invitrogen, 1:200). The coverslips were then mounted on the glass slide with Prolong Glass Antifade Mounting Media.

To study the effect of LT-025, a 100 µg/mL solution of ADC was added to fresh complete medium was added to adhered cells on the coverslips and incubated for 24 h. Untreated cells were also taken in similar conditions to the control. After washing, the cells were fixed in 4% paraformaldehyde (Electron Microscopy Sciences), followed by permeabilization and blocking in PBS containing 5% goat serum and 0.3% Triton X for 1 h at room temperature. The primary antibody anti-α,β tubulin antibody (cell signaling technology, rabbit IgG, 1:50) was incubated for 16 h at 4 ºC. After washing, Alexa Fluor 488 secondary antibody (green, Invitrogen, anti-rabbit IgG,

1:500) in 1 % BSA and 0.3 % Triton X was added and incubated for 1 h. Further F-actin staining was carried out using Rhodamine-Phalloidin (red, Invitrogen, 1:400) for 1 h at room temperature. Finally, the nucleus staining was carried out using Hoechst (blue, Invitrogen, 1:200). The coverslips were then mounted on the glass slide with Prolong Glass Antifade Mounting Media. Imaging was done using either Zeiss LSM 800, Airyscan confocal laser scanner microscope with Zen 2.3 software. Postprocessing of the image was done in ImageJ v1.52a software.

Enzyme-linked immunosorbent assay (ELISA)

The antigen-binding ability of ADCs was studied by Enzyme-Linked Immuno-Sorbent Assay (ELISA). 50 µl solution 2 µg/mL solution (100 ng) of mouse KIM-1 (SinoBiological, 50321-M16H) in PBS was coated on an ELISA plate (ELISA Max, Biolegend) and incubated overnight at 4 ºC. The plate was washed using PBST three times for five minutes each. Then, 300 µl of 10% BSA was added for blocking and incubated at room temperature for 90 min. Later, 100 µl of LT-025 and KIM-1 antibody control was added in varied concentrations and incubated at 37 ºC for 1 h. After subsequent washing, HRP conjugated secondary antibody of IgG1 (1:1500 dilution) was added and incubated for 30 minutes at 37 ºC. TMB substrate was then added after multiple washes with PBST. After five minutes, 2 N H_2SO_4 was added to stop the reaction, and the absorbance was recorded at 450 nm, and the data was analyzed using GraphPad Prism. The dissociation constant K_d was calculated from the absorbance versus concentration plot fitted to a one-site specific binding equation using GraphPad Prism software.

Biolayer Interferometry

Octet RH16 (previously Octet 698 RED384) from Sartorius was used for the BLI measurement. The analysis was carried out in a 699 Octet Red 384-well plate. PBS with 0.05% Tween 20 (PBST) was used for the hydration of the streptavidin sensor. The sensors were hydrated for two minutes before analysis. PBST was also used as the analysis buffer and for sample preparation to minimize all possible non-specific interactions. Mouse-KIM-1 antigen (SinoBiological, 50321-M16H) was biotinylated using Thermo Scientific EZ-Link™ Micro Sulfo-NHS-LC-Biotinylation Kit. 10 µg/mL of biotinylated KIM-1 was used as the load. After the baseline setting for 120 seconds, loading was performed for 120 seconds, followed by another baseline setting for 120 seconds. The association and dissociation with the LT-025 samples were recorded for 600 seconds each. Negative control for sensors was carried out without loading the biotinylated protein, and a null concentration of samples was used as a negative control for the samples, and these responses were subtracted from the samples. The analysis of the result was carried out in Octet Analysis Studio 13.0. Inter-step correction was performed by aligning to the baseline step, and noise filtering was performed.

Stability of ADC

The stability of the ADC was determined using the HIC chromatography method. 1 mg/mL of LT-025 in mouse plasma was incubated at 4 ºC and room temperature. 10 µL of each sample was injected into the HPLC connected to the HIC. The area under the curve of the peak corresponding to the ADC was measured and plotted for different days.

DAR calculation

The DAR of LT-025 was calculated using UV-visible spectroscopy. First, the extinction coefficient of both the antibody and the linker was calculated using Beer-Lambert's law with a known concentration. Then the concentration of antibody part (C_{mAb}) and drug-linker part (C_{drug}) of the ADC was calculated using equations 1, and 2, and DAR was calculated using equation 3.

$$C_{mAb} = (A_{280}\varepsilon_{drug}^{\lambda(D)} - A_{\lambda(D)}\,\varepsilon_{drug}^{\lambda(D)})/[\left(\varepsilon_{mAb}^{280}\,\varepsilon_{drug}^{\lambda(D)} - \varepsilon_{mAb}^{\lambda(D)}\,\varepsilon_{drug}^{280}\right)l] \qquad \text{Equation 1}$$

$$C_{drug} = (A_{280}\varepsilon_{mAb}^{\lambda(D)} - A_{\lambda(D)}\,\varepsilon_{mAb}^{\lambda(280)})/[\left(\varepsilon_{drug}^{280}\,\varepsilon_{mAb}^{\lambda(D)} - \varepsilon_{drug}^{\lambda(D)}\,\varepsilon_{mAb}^{280}\right)l] \qquad \text{Equation 2}$$

$$DAR = C_{drug}/C_{mAb} \qquad \text{Equation 3}$$

where, A_{280} is the absorbance of ADC at 280 nm, $\varepsilon_{drug}^{\lambda(D)}$ is the extinction coefficient of drug-linker at 254 nm, $A_{\lambda(D)}$ is the absorbance of ADC at 254 nm, $\varepsilon_{drug}^{\lambda(D)}$ is the extinction coefficient of drug-linker 254 nm, ε_{mAb}^{280} is the extinction coefficient of antibody at 280 nm, $\varepsilon_{mAb}^{\lambda(D)}$ is the extinction coefficient of antibody at 254 nm, ε_{drug}^{280} is the extinction coefficient of drug-linker at 280 nm and l is the pathlength, which is 1 cm.

In-vitro cytotoxicity studies

Renca cells were seeded in a culture-treated 96-well plate (2.5 k cells per well) and incubated at 37 °C under 5% CO_2 for 24 h. The LT-025 sample was added in increasing concentration in the fresh media and incubated under the same conditions for 48 h. Further, the ADC-containing media were removed from the wells, and 0.5 mg/mL MTT dissolved in basal medium (100 µL) was added and incubated for 3 h. Later, the formazan crystals were dissolved in DMSO by replacing the MTT solution. The absorbance at 570 nm was read using a BioTek Epoch microplate reader. The IC_{50} values were then calculated by fitting the data with the logistic function to create a sigmoidal dose-response curve. All measurements were performed in triplicate. Data were analyzed by Prism 10 (GraphPad) software.

Generation of Renca$^{KIM-1++}$ by overexpressing KIM-1

We have used lentiviral transduction of wild-type Renca cells to overexpress KIM-1. HAVCR-1 Mouse tagged ORF Clone Lentiviral particle (MR203831L3V, Origene, Rockville, MD) containing the desired murine-KIM-1/ HAVCR1 gene along with a puromycin-resistant gene for selection, was used to transfect mouse renal adenocarcinoma cells (Renca). The transduction of lentivirus was performed according to the manufacturer's protocol. A similar lentivirus with the same ORF but lacking the KIM-1 gene (PS100092V) was used as a negative control. Antibiotic selection using 0.5 µg/mL puromycin in complete RPMI medium was performed (according to the manufacturer's recommendation) to enrich the Renca$^{KIM-1++}$ population. The concentration of puromycin was determined by generating a kill-curve using MTT assay with the transduced Renca cells. The KIM-1 expression in Renca$^{KIM-1++}$ was investigated using western blot and flow cytometric analysis.

Western blot

Normal Renca and Renca$^{KIM-1++}$ cells were seeded in a 6-well plate at a density of 600k cells per well and incubated at 37 °C under 5% CO_2 for 16 h. The Cells were lysed with RIPA lysis buffer supplemented with protease and phosphatase inhibitors for 30 min at 4 °C with mild vortexing every 10-15 min, followed by

centrifugation. The amount of protein was optimized by bicinchoninic acid assay (Thermo Scientific) according to the manufacturer's protocol. 40 µg of protein lysates were electrophoresed on a 10% polyacrylamide gel at 80-120 V until resolved completely. The proteins were transferred to an Immun-Blot PVDF membrane (Biorad, 0.2 µm) through wet blotting for 3 h at 300 mA. Membranes were blocked by either 5% non-fat dry milk in TBS-T (TBS containing 0.1% Tween-20) or 5% BSA in 1x TBS-T for 1h and incubated with appropriate primary antibodies at 4 °C for 16-18 h. After that, the membrane was washed 3 times with 1x TBS-T. Then the membrane was incubated with secondary antibody HRP-goat-anti-mouse/rabbit (1:1000) (BioRad) for 1 h at room temperature. The membranes were washed two times with 1xTBS-T and one time with TBS before being developed using femto chemiluminescent substrate (Thermo Scientific) and imaged using Biorad ChemiDOC XRS+ using Image Lab version 6.1 image analysis. The antibodies used for the western blot analysis are anti-mouse-KIM-1 antibody (Abcam, rabbit polyclonal, 1:500), E-Cadherin (Cell Signaling Technology, Cat. No. 3195, 1:1000), or GAPDH (Cell Signaling Technology, 1:1000)

For the study of expression of E-cadherin, different concentrations of LT-025 from 0 nM to 500 nM were treated to 600k cells adhered on 6-well plates in fresh complete media for 24 h. After the treatment, the media was removed and prepared the lysate and carried out western blotting according to the same protocol mentioned above.

Development of sunitinib-resistant cells and apoptosis assay

For the development of sunitinib-resistant Renca cells, the parental cells were continuously treated with sunitinib in increasing concentrations of sunitinib from 1 µM, 2.5 µM, 5 µM, 6 µM, 7.5 µM, 8.5 µM, 10 µM to 12.5 µM. The cells were allowed to grow in sunitinib-containing media until they were confluent. Then the cells were splitted to two flask: one with the same concentration of sunitinib where the cells were already in, and another with the higher dose. The cells followed a pattern of getting confluency in 4 days, and the treatment continued for one month. After the dose of 12.5 µM of sunitinib, the growth of cells was reduced considerably, which is a characteristic of resistant cells.

For the apoptotic assay, 100 k of these sunitinib-resistant cells and normal Renca cells were treated with 100 nM of LT-025, 12.5 µM of sunitinib, and a combination of both for 24 hours in a 24-well plate. The cells were collected, washed, and stained with Annexin V-AF645 (Invitrogen, A23204) for 15 minutes at RT. The cells were then diluted with 200 µl of binding buffer and run on the flow cytometry with Novocyte flow cytometry. The analysis was carried out using FlowJo 10.10.0, and the data were plotted in GraphPad Prism.

In vivo dose escalation study

We have performed a dose escalation study in 10 male balb/c mice (8-10 weeks old, Charles River Laboratories, Strain Code 028). The LT-025 was administered by i.v. injection at the dose of 0.83 mg/kg to 3.33 mg/kg at an interval of 3-4 days. The mice were monitored for their weight and normal movement to evaluate any signs of toxicity. We have sacrificed 5 animals after the 1.67 mg/kg dose and the remaining 5 after the 3.33 mg/kg dose. We have collected blood from each mouse by intracardiac puncture and performed detailed blood biochemistry analysis for critical components representative of any systemic toxicity.

In vivo tumor reduction studies

Renca cells (1×10^6 cells in PBS) were injected subcutaneously into flank region of 8-10 weeks syngeneic male balb/c mice (Charles River Laboratories, Strain Code 028). The animals were randomized into four different

treatment groups once the tumor size is in between ~50 - 100 mm^3. Each group has 5 animals. LT-025 was administered at the dose of 1.67 mg/kg via the tail vein. Sunitinib (20 mg/kg) was given orally in a formulation with N-carboxymethyl cellulose and Tween 80. The drug administration was followed according to the schedule in Fig.6c. The mice's weight and tumor volume were monitored every other day.

The tumor volume was calculated using **Equation 4**:

$$V = \frac{W^2 \cdot L}{2}$$

where V, W, and L are the tumor volume and the shortest and the longest diameter, respectively, as measured using a vernier caliper. The animals were euthanized when it almost reached the permissive tumor volume. The blood samples were collected for serum toxicity analysis on the day of euthanasia. All procedures were performed according to the approved animal protocol by the BWH Institutional Use and Care of Animals Committee.

Statistical analysis

All statistical analysis was performed using Prism 10 (GraphPad) software. Experimental data were expressed as means ± SEM (otherwise specifically stated), and a *t*-test or one- or two-way analysis of variance (ANOVA) followed by an appropriate post-test was used to calculate statistical significance. $P < 0.05$ was considered significant and represented as *. Other P values were represented as $^{**}P < 0.01$, $^{***}P < 0.001$, and $^{****}P < 0.0001$.

ACKNOWLEDGMENTS

We acknowledge the Harvard Center for Mass Spectrometry for the guidance on data acquisition and analysis.

Funding: This work was supported by the U.S. Army Medical Research Acquisition Activity [W81XWH2210619 (T.S.)], Melanoma Research Alliance [2022A015448 (T.S.)], NIH-National Cancer Institute [R01CA276525 (S.S.)].

Author contributions: Conceptualization: T.S., Methodology: L.T., K.V., B.S., and A.K. Investigation: L.T., K.V., B.S., A.K., and T.S. Supervision: T.S. and S.S. Writing—original draft: T.S., and L.T. Writing—review and editing: T.S., L.T., and S.S.

Competing interests: S.S. is a co-founder and owns equity in Vyome Therapeutics, Akamara Therapeutics, and Invictus Oncology, and receives fees from Famygen and Advamedica. The other authors declare that they have no competing interests.

REFERENCE

1 Kidney cancer, Key statistics about kidney cancer, American Cancer Society.

2 Young, M. *et al.* Renal cell carcinoma. *The Lancet* **404**, 476-491 (2024). https://doi.org/https://doi.org/10.1016/S0140-6736(24)00917-6

3 Kidney Cancer Treatment, American Cancer Society.

4 Cardenas, L. M., Sigurdson, S., Wallis, C. J. D., Lalani, A. K. & Swaminath, A. Advances in the management of renal cell carcinoma. *Cmaj* **196**, E235-e240 (2024). https://doi.org/10.1503/cmaj.230356

5 Padala, S. A. *et al. Epidemiology of Renal Cell Carcinoma*. (2020).

6 Posadas, E. M., Limvorasak, S. & Figlin, R. A. Targeted therapies for renal cell carcinoma. *Nature Reviews Nephrology* **13**, 496-511 (2017). https://doi.org/10.1038/nrneph.2017.82

7 Escudier, B. *et al.* Sorafenib in advanced clear-cell renal-cell carcinoma. *N Engl J Med* **356**, 125-134 (2007). https://doi.org/10.1056/NEJMoa060655

8 Motzer, R. J., Escudier, B., Gannon, A. & Figlin, R. A. Sunitinib: Ten Years of Successful Clinical Use and Study in Advanced Renal Cell Carcinoma. *The Oncologist* **22**, 41-52 (2017). https://doi.org/10.1634/theoncologist.2016-0197

9 Tran, J. & Ornstein, M. C. Clinical Review on the Management of Metastatic Renal Cell Carcinoma. *JCO Oncology Practice* **18**, 187-196 (2022). https://doi.org/10.1200/op.21.00419

10 Yao, C., Zhang, T., Wu, T. & Brugarolas, J. Facts and Hopes for Immunotherapy in Renal Cell Carcinoma. *Clinical Cancer Research* **28**, 5013-5020 (2022). https://doi.org/10.1158/1078-0432.Ccr-21-2372

11 Rini, B. I. *et al.* Pembrolizumab plus axitinib versus sunitinib for advanced clear cell renal cell carcinoma: 5-year survival and biomarker analyses of the phase 3 KEYNOTE-426 trial. *Nature Medicine* **31**, 3475-3484 (2025). https://doi.org/10.1038/s41591-025-03867-5

12 Kapoor, A. First-line treatment options in metastatic renal cell cancer. *Can Urol Assoc J* **10**, S236-s238 (2016). https://doi.org/10.5489/cuaj.4307

13 Shah, N. J. *et al.* Health Care Resource Use for Modern First-Line Treatments in Metastatic Renal Cell Carcinoma. *JAMA Network Open* **7**, e2422674-e2422674 (2024). https://doi.org/10.1001/jamanetworkopen.2024.22674

14 Tsuchikama, K., Anami, Y., Ha, S. Y. Y. & Yamazaki, C. M. Exploring the next generation of antibody–drug conjugates. *Nature Reviews Clinical Oncology* **21**, 203-223 (2024). https://doi.org/10.1038/s41571-023-00850-2

15 Flynn, P., Suryaprakash, S., Grossman, D., Panier, V. & Wu, J. The antibody-drug conjugate landscape. *Nat Rev Drug Discov* **23**, 577-578 (2024). https://doi.org/10.1038/d41573-024-00064-w

16 Zhou, W. *et al.* Landscape of clinical drug development of ADCs used for the pharmacotherapy of cancers: an overview of clinical trial registry data from 2002 to 2022. *BMC Cancer* **24**, 898 (2024). https://doi.org/10.1186/s12885-024-12652-5

17 Fu, Z., Li, S., Han, S., Shi, C. & Zhang, Y. Antibody drug conjugate: the "biological missile" for targeted cancer therapy. *Signal Transduction and Targeted Therapy* **7**, 93 (2022). https://doi.org/10.1038/s41392-022-00947-7

18 Sganga, S. *et al.* Antibody–Drug Conjugates for the Treatment of Renal Cancer: A Scoping Review on Current Evidence and Clinical Perspectives. *Journal of Personalized Medicine* **13**, 1339 (2023).

19 Mahmoud, A. M. *et al.* Antibody-Based Therapeutics for the Treatment of Renal Cell Carcinoma: Challenges and Opportunities. *Oncologist* **28**, 297-308 (2023). https://doi.org/10.1093/oncolo/oyac263

20 Sugai, A., Miyai, K., Ito, K., Matsukuma, S. & Sato, K. Kidney Injury Molecule-1 Expression in Pathological T1b Clear Cell Renal Cell Carcinoma: A Putative Biomarker of High Immune-Inflamed Status and Recurrence. *Pathol Int* **75**, 340-348 (2025). https://doi.org/10.1111/pin.70024

21 Zhang, P. L. *et al.* Urine kidney injury molecule-1: a potential non-invasive biomarker for patients with renal cell carcinoma. *Int Urol Nephrol* **46**, 379-388 (2014). https://doi.org/10.1007/s11255-013-0522-z

22 Lin, F. *et al.* Human kidney injury molecule-1 (hKIM-1): a useful immunohistochemical marker for diagnosing renal cell carcinoma and ovarian clear cell carcinoma. *Am J Surg Pathol* **31**, 371-381 (2007). https://doi.org/10.1097/01.pas.0000213353.95508.67

23 Bonventre, J. V. Kidney injury molecule-1: a translational journey. *Trans Am Clin Climatol Assoc* **125**, 293-299; discussion 299 (2014).

24 Thomas, L. J. *et al.* Development of a Novel Antibody-Drug Conjugate for the Potential Treatment of Ovarian, Lung, and Renal Cell Carcinoma Expressing TIM-1. *Mol Cancer Ther* **15**, 2946-2954 (2016). https://doi.org/10.1158/1535-7163.Mct-16-0393

25 McGregor, B. A. *et al.* Safety and efficacy of CDX-014, an antibody-drug conjugate directed against T cell immunoglobulin mucin-1 in advanced renal cell carcinoma. *Invest New Drugs* **38**, 1807-1814 (2020). https://doi.org/10.1007/s10637-020-00945-y

26 Wang, R. *et al.* Antibody–Drug Conjugates (ADCs): current and future biopharmaceuticals. *Journal of Hematology & Oncology* **18**, 51 (2025). https://doi.org/10.1186/s13045-025-01704-3

27 Aoyama, M. *et al.* Linker and Conjugation Site Synergy in Antibody–Drug Conjugates: Impacts on Biological Activity. *Bioconjugate Chemistry* **35**, 1568-1576 (2024). https://doi.org/10.1021/acs.bioconjchem.4c00348

28 Strop, P. *et al.* Site-specific conjugation improves therapeutic index of antibody drug conjugates with high drug loading. *Nature Biotechnology* **33**, 694-696 (2015). https://doi.org/10.1038/nbt.3274

29 Pillow, T. H. *et al.* Site-Specific Trastuzumab Maytansinoid Antibody–Drug Conjugates with Improved Therapeutic Activity through Linker and Antibody Engineering. *Journal of Medicinal Chemistry* **57**, 7890-7899 (2014). https://doi.org/10.1021/jm500552c

30 Zhang, P. L. *et al.* Urine kidney injury molecule-1: a potential non-invasive biomarker for patients with renal cell carcinoma. *International Urology and Nephrology* **46**, 379-388 (2014). https://doi.org/10.1007/s11255-013-0522-z

31 Scelo, G. *et al.* KIM-1 as a Blood-Based Marker for Early Detection of Kidney Cancer: A Prospective Nested Case–Control Study. *Clinical Cancer Research* **24**, 5594-5601 (2018). https://doi.org/10.1158/1078-0432.Ccr-18-1496

32 Scelo, G. *et al.* KIM-1 as a Blood-Based Marker for Early Detection of Kidney Cancer: A Prospective Nested Case-Control Study. *Clin Cancer Res* **24**, 5594-5601 (2018). https://doi.org/10.1158/1078-0432.Ccr-18-1496

33 Lewis Phillips, G. D. *et al.* Targeting HER2-Positive Breast Cancer with Trastuzumab-DM1, an Antibody–Cytotoxic Drug Conjugate. *Cancer Research* **68**, 9280-9290 (2008). https://doi.org/10.1158/0008-5472.Can-08-1776

34 Dumontet, C., Reichert, J. M., Senter, P. D., Lambert, J. M. & Beck, A. Antibody–drug conjugates come of age in oncology. *Nature Reviews Drug Discovery* **22**, 641-661 (2023). https://doi.org/10.1038/s41573-023-00709-2

35 Anami, Y. & Tsuchikama, K. Transglutaminase-Mediated Conjugations. *Methods Mol Biol* **2078**, 71-82 (2020). https://doi.org/10.1007/978-1-4939-9929-3_5

36 Sadiki, A. *et al.* Site-Specific Conjugation of Native Antibody: Transglutaminase-Mediated Modification of a Conserved Glutamine While Maintaining the Primary Sequence and Core Fc Glycan via Trimming with an Endoglycosidase. *Bioconjugate Chemistry* **35**, 465-471 (2024). https://doi.org/10.1021/acs.bioconjchem.4c00013

37 Dennler, P. *et al.* Transglutaminase-Based Chemo-Enzymatic Conjugation Approach Yields Homogeneous Antibody–Drug Conjugates. *Bioconjugate Chemistry* **25**, 569-578 (2014). https://doi.org/10.1021/bc400574z

38 Dickgiesser, S. *et al.* Site-Specific Conjugation of Native Antibodies Using Engineered Microbial Transglutaminases. *Bioconjugate Chemistry* **31**, 1070-1076 (2020). https://doi.org/10.1021/acs.bioconjchem.0c00061

39 Gupta, N. *et al.* Computationally designed antibody–drug conjugates self-assembled via affinity ligands. *Nature Biomedical Engineering* **3**, 917-929 (2019). https://doi.org/10.1038/s41551-019-0470-8

40 Hamblett, K. J. *et al.* Effects of drug loading on the antitumor activity of a monoclonal antibody drug conjugate. *Clin Cancer Res* **10**, 7063-7070 (2004). https://doi.org/10.1158/1078-0432.Ccr-04-0789

41 Ge, J. *et al.* TRBC2-targeting antibody–drug conjugates for the treatment of T cell cancers. *Nature Cancer* **6**, 2011-2024 (2025). https://doi.org/10.1038/s43018-025-01069-z

42 Lopus, M. *et al.* Maytansine and Cellular Metabolites of Antibody-Maytansinoid Conjugates Strongly Suppress Microtubule Dynamics by Binding to Microtubules. *Molecular Cancer Therapeutics* **9**, 2689-2699 (2010). https://doi.org/10.1158/1535-7163.Mct-10-0644

43 VUORINEN, R.-L. *et al.* Sunitinib First-line Treatment in Metastatic Renal Cell Carcinoma: Costs and Effects. *Anticancer Research* **39**, 5559-5564 (2019). https://doi.org/10.21873/anticanres.13749

44 Motzer, R. J. *et al.* Pazopanib versus Sunitinib in Metastatic Renal-Cell Carcinoma. *New England Journal of Medicine* **369**, 722-731 (2013). https://doi.org/doi:10.1056/NEJMoa1303989

45 Schmid, T. A. & Gore, M. E. Sunitinib in the treatment of metastatic renal cell carcinoma. *Therapeutic Advances in Urology* **8**, 348-371 (2016). https://doi.org/10.1177/1756287216663979

46 Ghosh, S. *et al.* Impact of sunitinib resistance on clear cell renal cell carcinoma therapeutic sensitivity in vitro. *Cell Cycle* **23**, 43-55 (2024). https://doi.org/10.1080/15384101.2024.2306760

47 Fontana, A., Spolaore, B., Mero, A. & Veronese, F. M. Site-specific modification and PEGylation of pharmaceutical proteins mediated by transglutaminase. *Adv Drug Deliv Rev* **60**, 13-28 (2008). https://doi.org/10.1016/j.addr.2007.06.015

48 Krapp, S., Mimura, Y., Jefferis, R., Huber, R. & Sondermann, P. Structural analysis of human IgG-Fc glycoforms reveals a correlation between glycosylation and structural integrity. *J Mol Biol* **325**, 979-989 (2003). https://doi.org/10.1016/s0022-2836(02)01250-0

49 Feige, M. J. *et al.* Structure of the murine unglycosylated IgG1 Fc fragment. *J Mol Biol* **391**, 599-608 (2009). https://doi.org/10.1016/j.jmb.2009.06.048

50 Ouyang, J. in *Antibody-Drug Conjugates* (ed Laurent Ducry) 275-283 (Humana Press, 2013).

51 Wynn, C., Patel, R., Hillegass, W. B. & Tang, S.-C. Increased systemic toxicities from antibody-drug conjugates (ADCs) with cleavable versus non-cleavable linkers: A meta-analysis of commercially available ADCs. *Journal of Clinical Oncology* **40**, 3032-3032 (2022). https://doi.org/10.1200/JCO.2022.40.16_suppl.3032

52 Lambert, J. M. & Chari, R. V. Ado-trastuzumab Emtansine (T-DM1): an antibody-drug conjugate (ADC) for HER2-positive breast cancer. *J Med Chem* **57**, 6949-6964 (2014). https://doi.org/10.1021/jm500766w

53 Staudacher, A. H. & Brown, M. P. Antibody drug conjugates and bystander killing: is antigen-dependent internalisation required? *British Journal of Cancer* **117**, 1736-1742 (2017). https://doi.org/10.1038/bjc.2017.367

54 Junttila, T. T., Li, G., Parsons, K., Phillips, G. L. & Sliwkowski, M. X. Trastuzumab-DM1 (T-DM1) retains all the mechanisms of action of trastuzumab and efficiently inhibits growth of lapatinib insensitive breast cancer. *Breast Cancer Res Treat* **128**, 347-356 (2011). https://doi.org/10.1007/s10549-010-1090-x

55 Motzer, R. J. *et al.* Activity of SU11248, a Multitargeted Inhibitor of Vascular Endothelial Growth Factor Receptor and Platelet-Derived Growth Factor Receptor, in Patients With Metastatic Renal Cell Carcinoma. *Journal of Clinical Oncology* **24**, 16-24 (2006). https://doi.org/10.1200/jco.2005.02.2574

56 Faivre, S., Demetri, G., Sargent, W. & Raymond, E. Molecular basis for sunitinib efficacy and future clinical development. *Nature Reviews Drug Discovery* **6**, 734-745 (2007). https://doi.org/10.1038/nrd2380

57 Motzer, R. J. *et al.* Sunitinib in Patients With Metastatic Renal Cell Carcinoma. *JAMA* **295**, 2516-2524 (2006). https://doi.org/10.1001/jama.295.21.2516

58 Molina, A. M. *et al.* Sunitinib objective response in metastatic renal cell carcinoma: Analysis of 1059 patients treated on clinical trials. *European Journal of Cancer* **50**, 351-358 (2014). https://doi.org/https://doi.org/10.1016/j.ejca.2013.08.021

59 Rini, B. I. & Atkins, M. B. Resistance to targeted therapy in renal-cell carcinoma. *The Lancet Oncology* **10**, 992-1000 (2009). https://doi.org/https://doi.org/10.1016/S1470-2045(09)70240-2

60 Jin, J. *et al.* Sunitinib resistance in renal cell carcinoma: From molecular mechanisms to predictive biomarkers. *Drug Resistance Updates* **67**, 100929 (2023). https://doi.org/https://doi.org/10.1016/j.drup.2023.100929

61 Wang, Y. *et al.* Mechanisms of sunitinib resistance in renal cell carcinoma and associated opportunities for therapeutics. *Br J Pharmacol* **180**, 2937-2955 (2023). https://doi.org/10.1111/bph.16252

62 Zhang, Q. *et al.* Decoding sunitinib resistance in ccRCC: Metabolic-reprogramming-induced ABAT and GABAergic system shifts. *iScience* **27**, 110415 (2024). https://doi.org/10.1016/j.isci.2024.110415

63 Patel, P. H., Senico, P. L., Curiel, R. E. & Motzer, R. J. Phase I study combining treatment with temsirolimus and sunitinib malate in patients with advanced renal cell carcinoma. *Clin Genitourin Cancer* **7**, 24-27 (2009). https://doi.org/10.3816/CGC.2009.n.004

64 Molina, A. M. *et al.* Phase 1 trial of everolimus plus sunitinib in patients with metastatic renal cell carcinoma. *Cancer* **118**, 1868-1876 (2012). https://doi.org/10.1002/cncr.26429

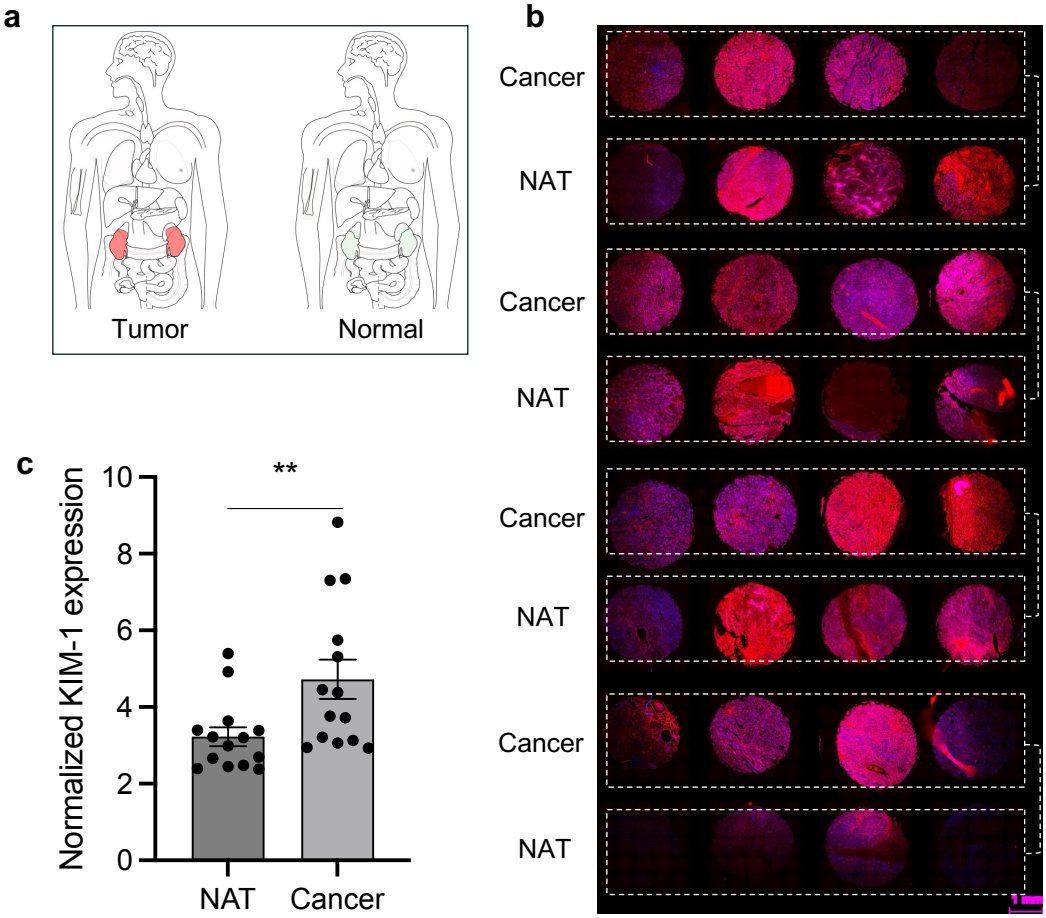

Figure 1: (**a**) Median expression of the KIM-1 gene in different cancer and normal tissues obtained from the TCGA dataset using Gene Expression Profiling Interactive Analysis (GEPIA). Inset: The pictorial representation of the KIM-1 expression in cancer (red) and normal (green) organs. The figure was generated using the GEPIA platform. (**b**) Immunostaining of kidney tissue microarray by anti-KIM-1 (red) antibody, and DAPI (blue). Tissue specimens were collected from randomized patients based on age, sex, and stage of cancer. The normal adjacent tissue (NAT) and tumor tissue were collected from the same patients. The image shows the majority of the tumor expressing high KIM-1. 16 such images were combined to form a single circular tissue image. (**c**) Bar plot showing relative KIM-1 expression in cancer and normal adjacent tissue (NAT). Each data point represents one patient sample. The data were represented as mean ± SEM (n = 16, paired t-test, $P < 0.01$ **).

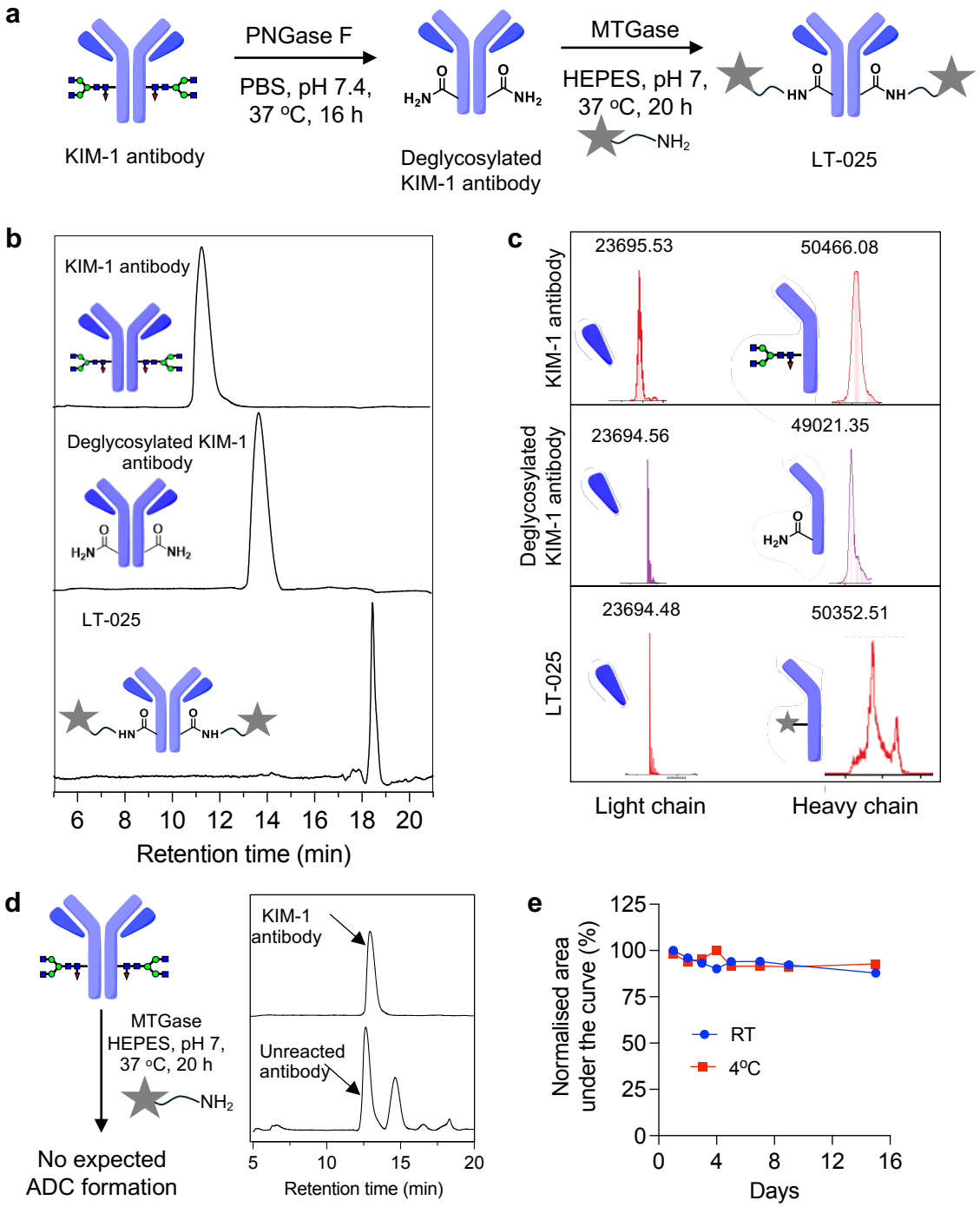

Figure 2: **Preparation and characterization of KIM-1 targeting ADC, LT-025**. (**a**) Schematic representation of the synthesis of KIM-1 targeting ADC, LT-025, by using transglutaminase. First, the native monoclonal KIM-1 antibody was deglycosylated in the presence of the PNGase F enzyme, and then the payload-linker was attached to the antibody at Q295 in the presence of the microbial transglutaminase enzyme (MTGase). The payload used was DM1. (**b**) Data shows the difference in the retention time of KIM-1 antibody, deglycosylated KIM-1 antibody, and ADC (LT-025) using hydrophobic interaction chromatography (HIC). Data was recorded under physiological conditions in PBS (pH 7.4) at 280 nm. 10 µg of each sample was injected for analysis. The chromatograms were baseline corrected using Origin 8.0 and plotted using GraphPad Prism 10 software. (**c**) Mass spectral analysis of the antibody drug conjugate. The data were recorded using ESI-MS after DTT reduction of the LT-025. Deconvoluted mass spectra of light chain and heavy chain, of KIM-1 antibody, deglycosylated KIM-1 antibody, and LT-025. 5 µg of each sample was injected for ESI-MS analysis. (**d**) The schematic shows the importance of the deglycosylation of the antibody for ADC production. The upper histogram represents the HIC chromatogram of the native antibody. The lower histogram is the product after the conjugation reaction without performing the deglycosylation step. The chromatogram shows the presence of unreacted antibody with some additional product, which does not match the desired LT-025 chromatogram. (**e**) The data represent the stability of the LT-025 for 15 days. The area under the curve from the HIC chromatogram of the ADC was normalized to day 1 and plotted with increasing days. 10 µL of 1 mg/mL of each sample was injected for analysis. The data shows no significant change in the peak area, indicating the stability of the ADC.

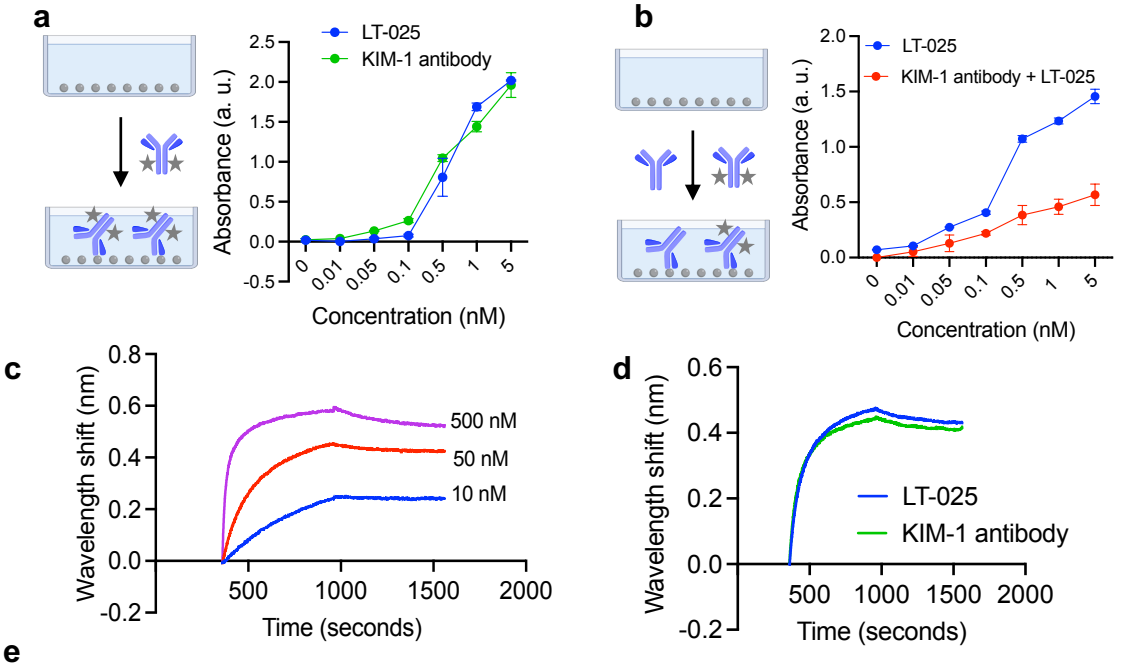

e

Sample	K_D (M)	K_D Error	k_a (1/Ms)	k_a Error	k_{dis} (1/s)	k_{dis} Error
LT-025	0.597×10^{-9}	8.51×10^{-12}	1.87×10^{5}	436	11.2×10^{-5}	1.57×10^{-6}
KIM-1 antibody	0.33×10^{-9}	8.6×10^{-12}	2.31×10^{5}	720.1	7.66×10^{-5}	1.98×10^{-6}

Figure 3. Biophysical characterization of the antigen recognition by LT-025. (**a**) The antigen-binding capacity of LT-025, and the KIM-1 antibody was studied using ELISA. The immobilization of the LT-025 was checked in a KIM-1 protein-coated ELISA plate. The presence of the LT-025 was measured using an HRP-conjugated secondary antibody. The data shows a dose-dependent increase in the absorption, representing the successful antigen binding by the LT-025. The antigen recognition of the LT-025 shows a similar dose response curve to that of the monoclonal KIM-1 antibody, signifying no loss of the antigen-binding capability of the ADC. (**b**) The comparison of the binding of LT-025 alone with ADC in the presence of KIM-1 free antibody was studied using ELISA. The data shows a 50% reduction in the immobilization of both ADC in the presence of free antibody. (**c**) Quantitative estimation of the antigen binding of the LT-025 using Bio-layer interferometry (BLI). The data shows dose-dependent increase in the association and dissociation events. (**d**) Comparison of the antigen binding of LT-025 and KIM-1 antibody using BLI. 50 nM of each sample was used for the study. (**e**) Equilibrium constants and rate constants of ADC and the antibody (K_D: Dissociation equilibrium constant, k_a: association rate constant, and k_{dis}: dissociation rate constant.

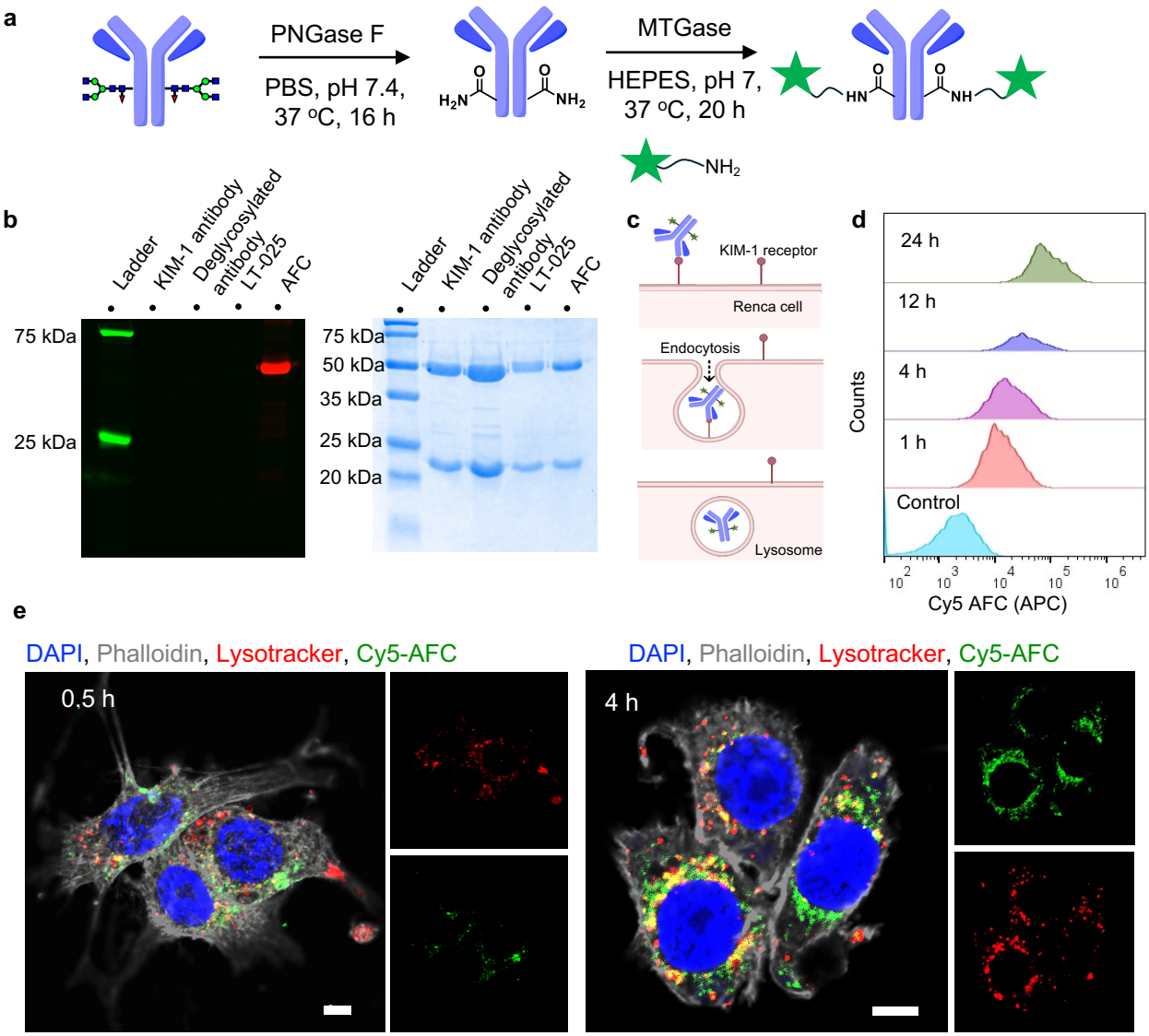

Figure 4: Cellular internalization by the antibody fluorophore conjugate (AFC). (**a**) Schematic representation of the synthesis of an antibody fluorophore conjugate (AFC) by using the MTGase reaction as described for the ADC. First, the native monoclonal antibody was deglycosylated in the presence of the PNGase F enzyme, and then the Cy5-fluorophore-linker was attached to the antibody at Q295 in the presence of the MTGase. (**b**) SDS-PAGE (fluorescence imaging and Coomassie staining) of KIM-1 antibody, deglycosylated antibody, LT-025, and Cy5-AFC. The data shows attachment of the Cy5 fluorophore in the heavy chain of the antibody. No conjugation of Cy5 was observed in the light chain. (**c**) Schematic representation of the cellular internalization of the ADC and AFC. The AFC first binds with the KIM-1 receptor on the cell surface, and it gets endocytosed into the cell and is transported to the lysosomal compartment. (**d**) Internalization study of Cy5 AFC at different time points. 50 µg/ml of AFC. An increase in MFI (Cy5) over time means increased binding/internalization of AFC onto the Renca RCC cell line. (**e**) Confocal microscopy images showing the internalization of the AFC in Renca cells. The images show successful cellular internalization of AFC (50 µg/ml) within 0.5 h and 4 h. An increased cellular internalization and colocalization at the lysosomal compartment were observed in 4 h. Scale bar = 5 µm.

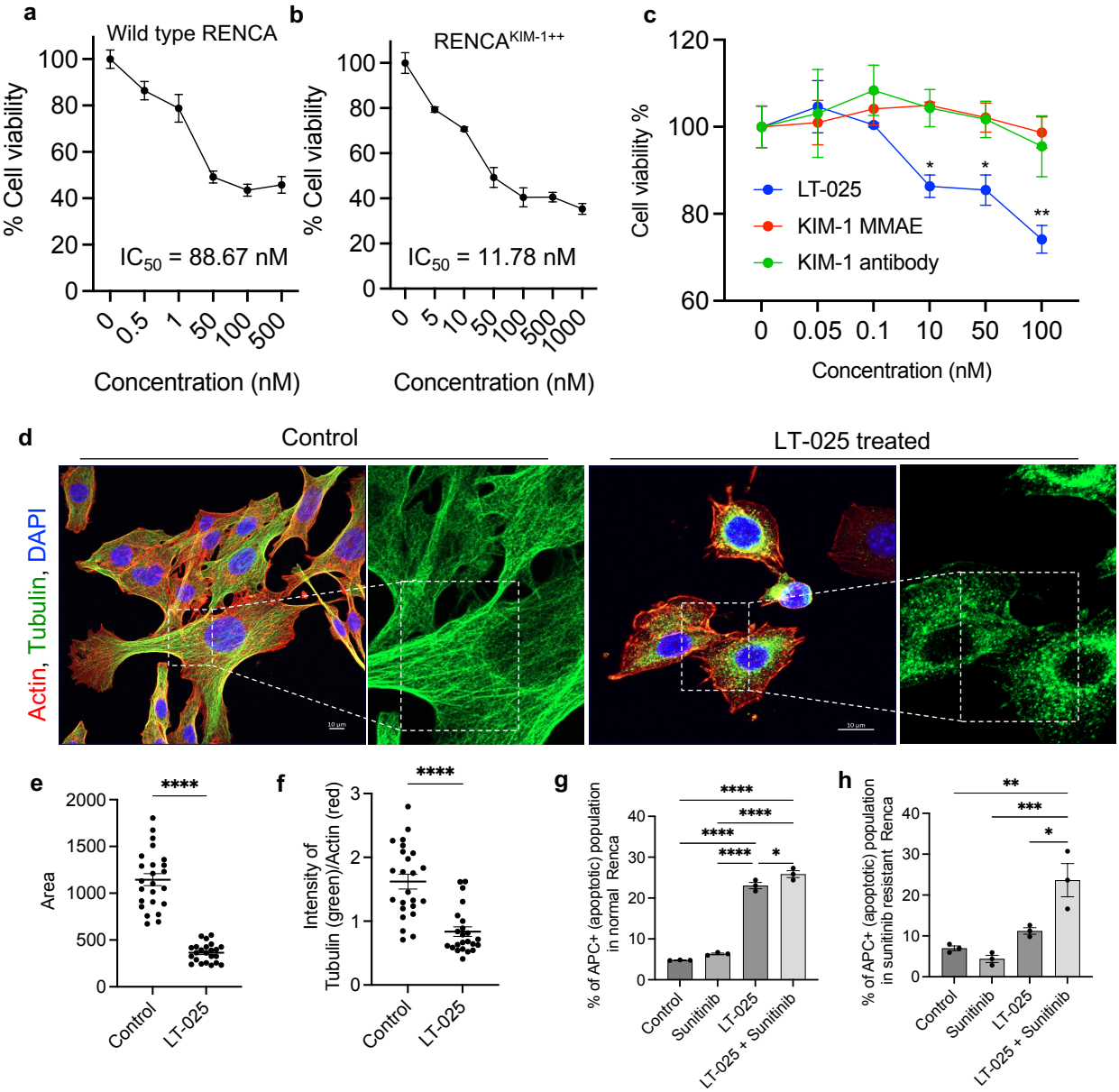

Figure 5: In vitro cytotoxic effect of LT-025. Cell viability and IC_{50} of ADC on (**a**) normal Renca and (**b**) Renca$^{KIM-1++}$, obtained by MTT assay. The LT-025 exhibits significant cell death with the IC_{50} values in the nanomolar range. A lower IC_{50} value was observed in Renca$^{KIM-1++}$ than in normal Renca because of increased receptor-mediated cellular internalization of the ADC. The data were represented as mean ± SEM (n = 3). (**c**) Comparison of the cell viability of LT-025, free antibody, and the KIM-1 MMAE ADC by MTT assay. The data showed significantly higher cell death by LT-025 in comparison to free KIM-1 antibody and KIM-1 MMAE ADC. The data were represented as mean ± SEM (n = 3, two-way ANOVA followed by Tukey's multiple comparison test). (**d**) Confocal images of Renca with and without treatment of LT-025 (100 µg/ml) displaying tubulin disruption. The images showed disruption of the tubulin (green) crosslinking by DM1, a known microtubule inhibitor. Sacale bar = 10 µm. (**e**) Quantification of tubulin in untreated and LT-025 treated cells from the confocal images. The mean pixel intensity of the tubulin (green) was plotted after normalizing with the mean pixel intensity of actin (red). The data were represented as mean ± SEM (n = 23, Unpaired *t*-test with Welch's correction). (**f**) Quantification of the area of the control and treated Renca cells. The data showed a significant reduction in the area of the cells. The data were represented as mean ± SEM (n = 23, Unpaired *t*-test with Welch's correction). (**g**) The bar plot showing the % of apoptotic cells measured with flow cytometry using Annexin-V AF645 apoptosis kit. The data represent significantly higher apoptosis in normal Renca by LT-025 compared to the control and sunitinib-treated group. (n = 3, one-way ANOVA followed by Tukey's multiple comparison test). (**h**) The bar plot showing the % of apoptotic sunitinib-resistant Renca measured with flow cytometry using Annexin V-AF645 apoptosis kit. The data represent significantly higher apoptosis in sunitinib-resistant Renca by treatment with dual therapy (LT-025 + sunitinib) compared to the control and monotherapy. 12.5 µM of sunitinib and 100 nM of ADC were used for the study (n = 3, one-way ANOVA followed by Tukey's multiple comparison test).

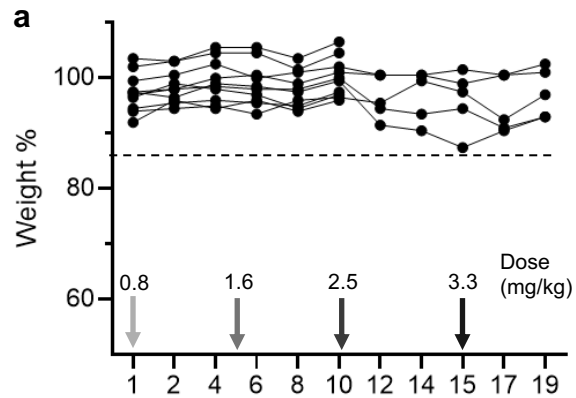

b

	Dose (1.6 mg/kg)	Dose (3.3 mg/kg)
ALP (U/L)	90.5 ± 6.50	91.25 ± 9.27
AST (U/L)	83 ± 11.67	81 ± 12.74
ALT (U/L)	37 ± 9.62	33 ± 3.05
Creatine kinase (U/L)	388 ± 114.6	403 ± 87.91
Total protein (g/dL)	5.6 ± 0.48	5.5 ± 0.40
Albumin (g/dL)	3.2 ± 0.2	3.15 ± 0.15
Globulin (g/dL)	2.4 ± 0.29	2.35 ± 0.27
Total bilirubin (mg/dL)	0.2 ± 0.05	0.2 ± 0.05
BUN (mg/dL)	18.5 ± 3.03	18.75 ± 4.39

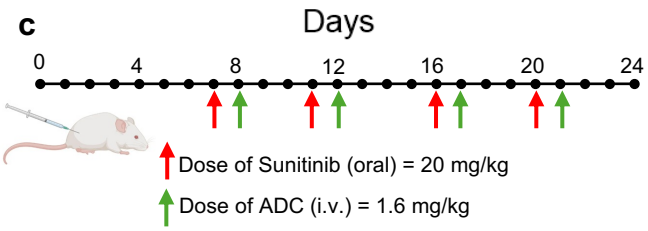

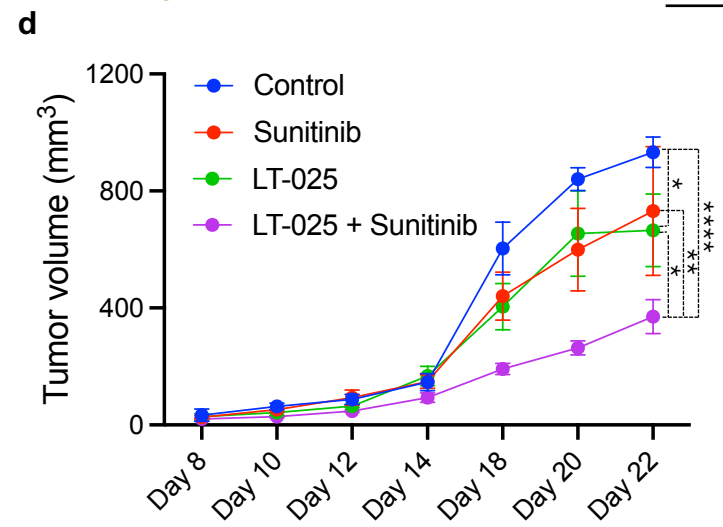

Figure 6: In vivo therapeutic efficacy of the LT-025. (**a**) Dose escalation study to evaluate any treatment-related toxicity. The data shows no significant change in the body weight of each mouse during the treatment. We sacrificed 5 mice after the 1.6 mg/kg dose to perform blood biochemistry analysis. No significant toxicity, i.e, no change of body weight more than 20% of the initial weight has been observed. (**b**) Blood biochemistry analysis from the dose escalation study after the doses of 1.6 and 3.3 mg/kg. The data show no abnormal levels of critical liver and kidney enzymes and blood components corresponding to safe treatment of the LT-025. (**c**) The schematic shows the study design for evaluating the therapeutic efficacy of LT-025 using a subcutaneous Renca tumor model in syngenic balb/c mice. The injection regime is indicated using red and green arrows. (**d**) Tumor growth curve showing the change in tumor volume of each treatment group. The data show a significant reduction in the tumor volume by LT-025. The therapeutic efficacy of LT-025 increases significantly in the presence of sunitinib compared to monotherapies. The data were represented as mean ± SEM (n = 5, two-way ANOVA followed by Tukey's multiple comparison test).

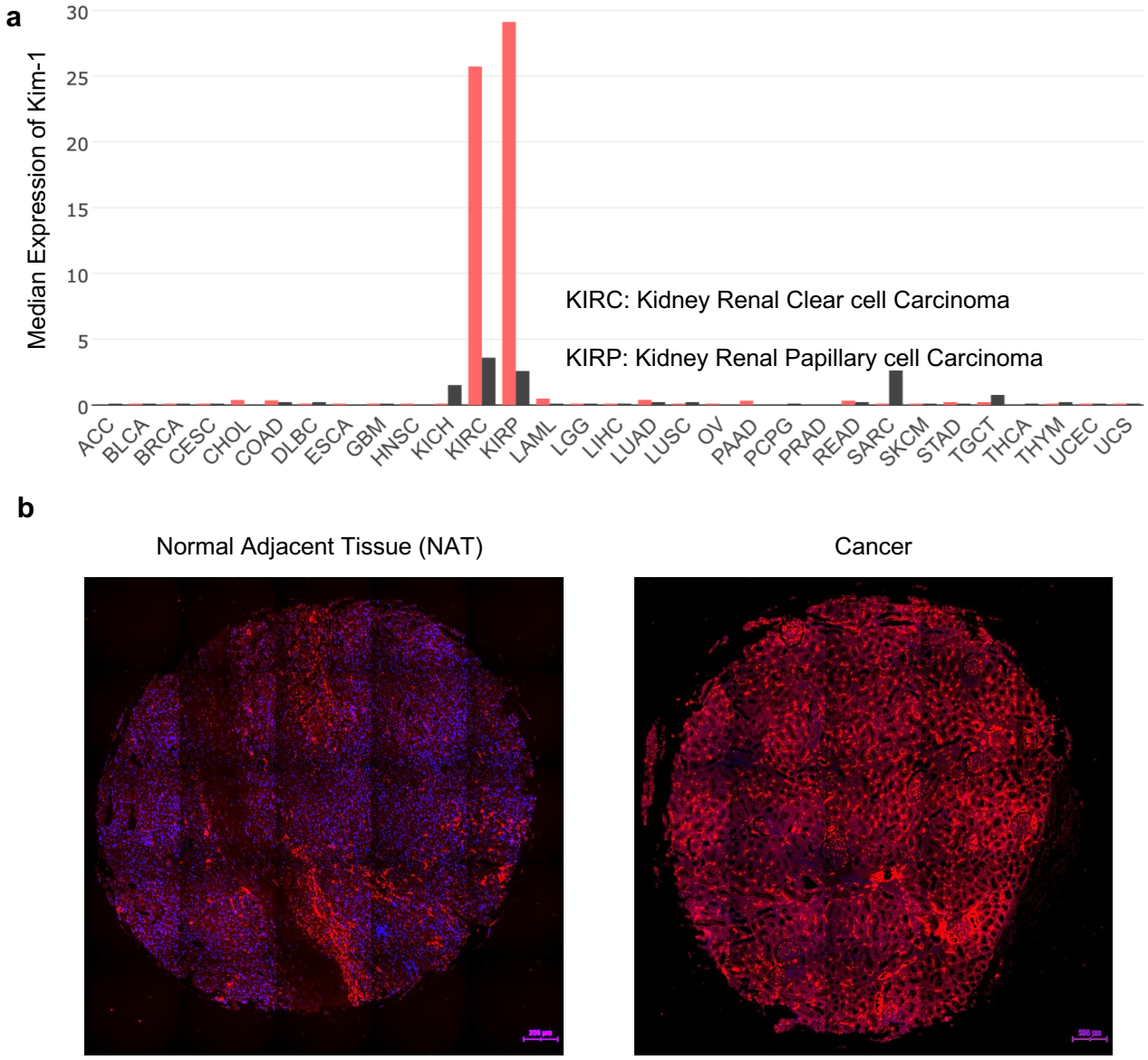

Supplementary Figure 1: (**a**) Median expression of the KIM-1 gene in different cancer and normal tissues obtained from the TCGA dataset using Gene Expression Profiling Interactive Analysis (GEPIA). (**b**) Representative images for immunostaining of kidney tissue microarray by anti-KIM-1 (red) antibody and DAPI (blue). Tissue specimens were collected from randomized patients based on age, sex, and stage of cancer. The normal adjacent tissue (NAT) and tumor tissue were collected from the same patients.

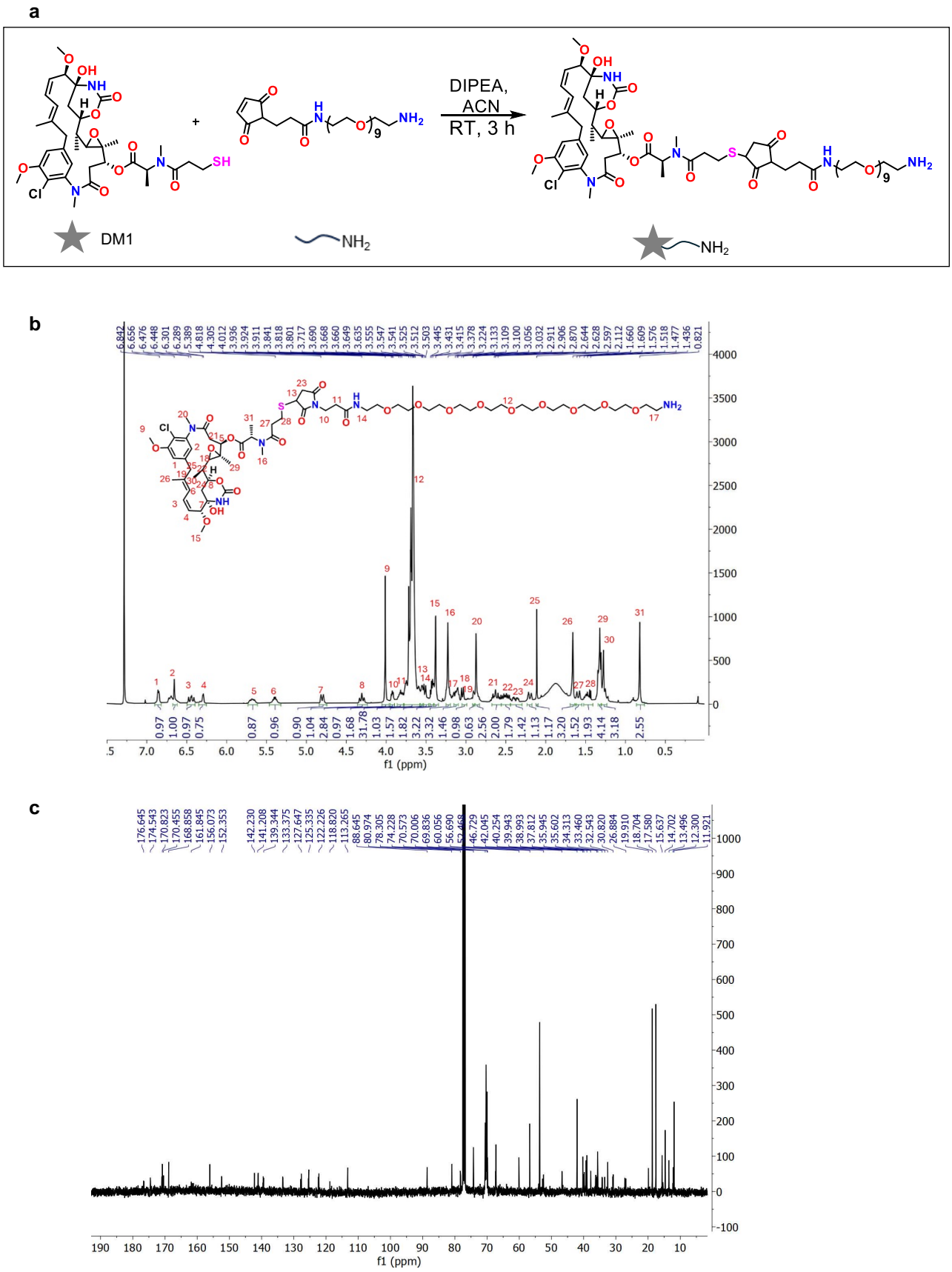

Supplementary Figure 2: Schematic representation of the DM1-linker preparation in a single step using DM1 and malamido-PEG$_9$ amine (DIPEA: N,N-Diisopropylethylamine, ACN: Acetonitrile, RT: Room temperature (**a**) and Characterization of the DM1-linker by ^{1}H NMR (**b**) and ^{13}C NMR (**c**).

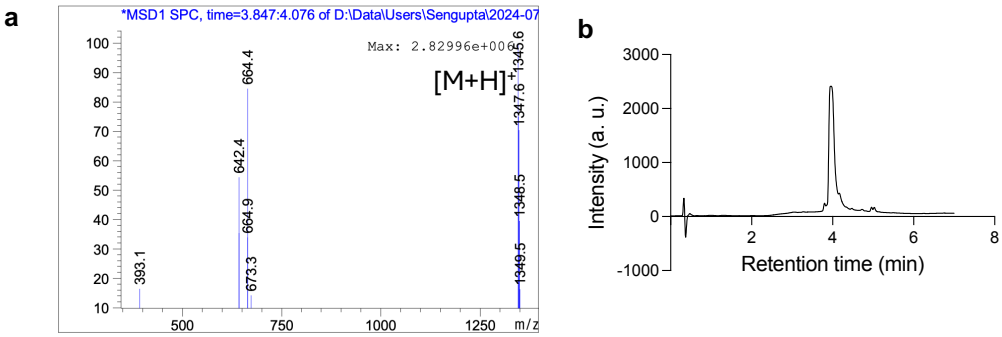

Supplementary Figure 3: (**a**) Mass spectral analysis of DM1 linker. Calculated mass for [M+H]+: 1345.6 Da, observed mass: 1345.6 Da. (**b**) RP-HPLC trace of DM1-linker representing the purity. A gradient method of 100 % water + 0.1 % formic acid to 100 % acetonitrile + 0.1 % formic acid was used for HPLC using a C18 column

a

Condition	Antibody : linker	Concentration of antibody	Buffer	Enzyme quantity
a	1:50	2 mg/ml	1:1 PBS+HEPES	2.5 eq
b	1:25	5 mg/ml	PBS	2.5 eq
c	1:50	2 mg/ml	1:2.5 PBS+HEPES	2.5 eq
d	1:100	10 mg/ml	HEPES	5 eq
e	1:50	5 mg/ml	1:1 PBS+HEPES	2.5 eq
f	1:50	5 mg/ml	1:2 PBS+HEPES	2.5 eq

b

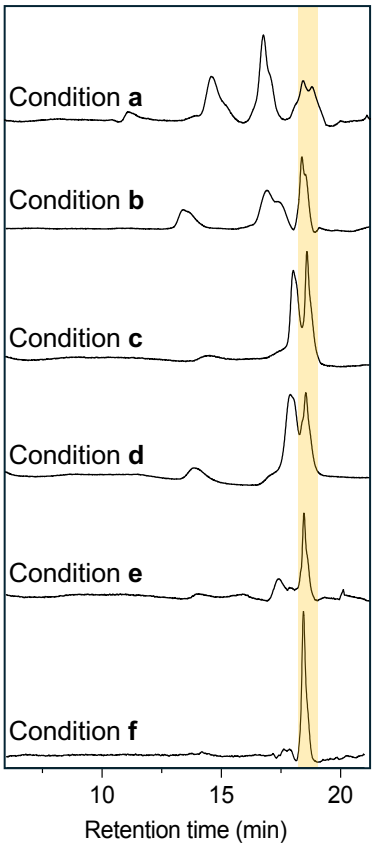

Supplementary Figure 4: (a) Optimization of reaction conditions for the synthesis of LT-025 using e-MTGase. **(b)** Hydrophobic interaction column chromatogram traces of product obtained in each reaction condition. Purification using MWCO filters was carried out before running the HPLC. 10 µL of 1 mg/mL of each sample was injected for analysis. Condition **f** corresponds to the chromatogram of LT-025. Method used for the HPLC is a gradient method from 100 % of 25 mM phosphate buffer pH 7 with 1.5 M ammonium sulphate to 100 % of 25 mM phosphate buffer pH 7 with 20 % isopropanol. The absorption was recorded at 280 nm. The chromatograms were baseline corrected using Origin 8.0 and were plotted using GraphPad Prism.

a

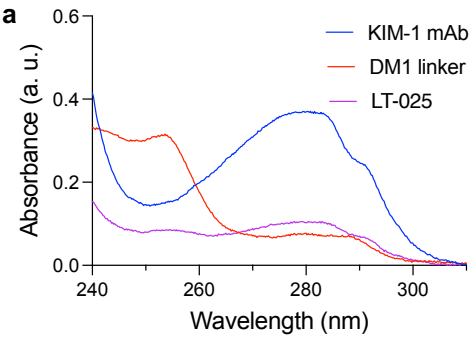

b

$$C_{mAb} = (A_{280}\,\varepsilon_{drug}{}^{\lambda(D)} - A_{\lambda(D)}\varepsilon_{drug}{}^{280})/[(\varepsilon_{mAb}{}^{280}\,\varepsilon_{drug}{}^{\lambda(D)} - \varepsilon_{mAb}{}^{\lambda(D)}\,\varepsilon_{drug}{}^{280})l]$$

$$C_{drug} = (A_{280}\,\varepsilon_{mAb}{}^{\lambda(D)} - A_{\lambda(D)}\varepsilon_{mAb}{}^{280})/[(\varepsilon_{drug}{}^{280}\,\varepsilon_{mAb}{}^{\lambda(D)} - \varepsilon_{dug}{}^{\lambda(D)}\,\varepsilon_{mAb}{}^{280})l]$$

$$DAR = Cdrug/CmAb$$

c

Conc of antibody	1.66E-06
Conc. of linker	1.70E-06
Absorbance of antibody at 280 nm	0.329
Absorbance of antibody at 254	0.134
Absorbance of linker at 280	0.09
Absorbance of linker at 254	0.35
Ext. coefficient of antibody at 280 nm ($\varepsilon_{mAb}{}^{280}$)	198192.771
Ext. coefficient of antibody at 254 nm ($\varepsilon_{mAb}{}^{\lambda(D)}$)	80722.8916
Ext. coefficient of linker at 280 nm ($\varepsilon_{drug}{}^{280}$)	1.94E+05
Ext. coefficient of linker at 254 ($\varepsilon_{drug}{}^{\lambda(D)}$)	2.06E+05
Absorbance of ADC at 280 (A_{280})	0.104
Absorbance of ADC at 254 ($A_{\lambda(D)}$)	0.085
Conc of antibody in ADC (C_{mAb})	1.97E-07
Conc of linker in ADC (C_{drug})	3.36E-07
DAR ($C_{drug}/CmAb$)	1.70E+00

Supplementary Figure 5: Calculation of DAR using UV-visible spectroscopy. **(a)** The absorption of spectra of LT-025, DM1 linker, and KIM-1 antibody are given. **(b)** The equation for the calculation of DAR. **(c)** Table showing the calculation of DAR using the equation by measuring the absorbance of the antibody and linker from the ADC. The extinction coefficients of the antibody and the linker were calculated by measuring the absorbance at known concentrations of antibody and linker. The absorption maxima of the linker and antibody were obtained as 254 nm, and 280 nm, respectively. The DAR was finally calculated by the ratio of C_{drug} to $C_{mAb.}$ Notation 'l' in the equation corresponds to the path length, which was considered as 1 cm.

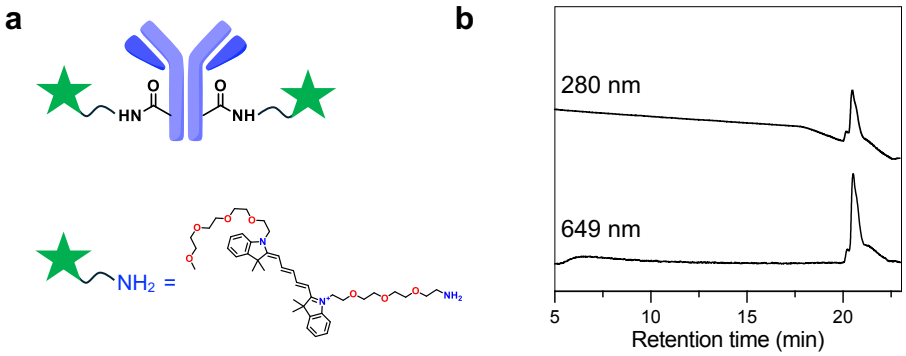

Supplementary Figure 6: (a) Schematic structure of KIM-1 Cy5 AFC and the structure of Cy5 linker **(b)** Characterization data of AFC using HIC. Method used for the HPLC is a gradient method from 100 % of 25 mM phosphate buffer pH 7 with 1.5 M ammonium sulphate to 100 % of 25 mM phosphate buffer pH 7 with 20 % isopropanol. The absorption was recorded at 280 nm and 649 nm (absorption maxima of Cy5 linker). The distinguished peak in the 649 nm chromatogram represents the presence of the Cy5 fluorophore in the AFC.

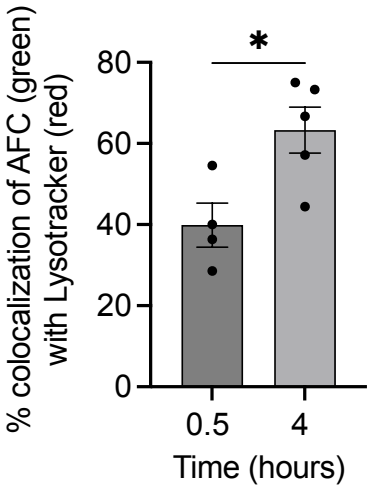

Supplementary Figure 7: Quantification of the colocalization between AFC (green) signal with Lysotracker (red) signal in Renca cells at 0.5 and 4 h. The data represent significantly higher colocalization at 4 h. The data were represented as mean ± SEM (n = 5, Unpaired *t*-test with Welch's correction).

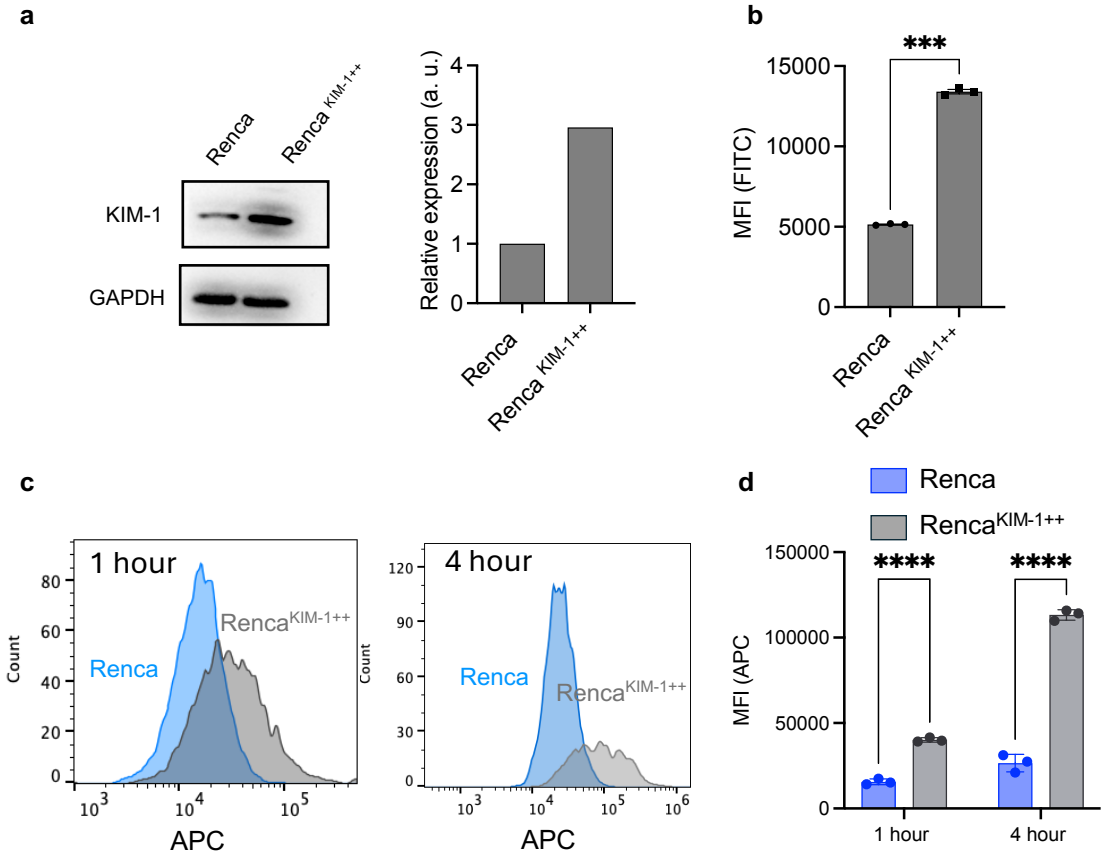

Supplementary Figure 8: Characterization of transduction of KIM-1 on RENCA cells using (**a**) Western blotting and (**b**) flow cytometry. The mean fluorescence intensity (MFI) was plotted in the bar graph. FITC conjugated anti-mouse KIM-1 antibody was used to probe the KIM-1 expression (**c**) The KIM-1 AFC internalization in Normal Renca and Renca$^{KIM-1++}$ by flow cytometry. The histogram shows a notable increase in the cellular internalization both at 1 and 4 h. (**d**) The bar graph represents the MFI of AFC internalization in Renca and Renca$^{KIM-1++}$ by flow cytometry. The data show a significant increase in cellular internalization. The data were represented as mean ± SEM (n = 3, two-way ANOVA followed by Tukey's multiple comparison test).

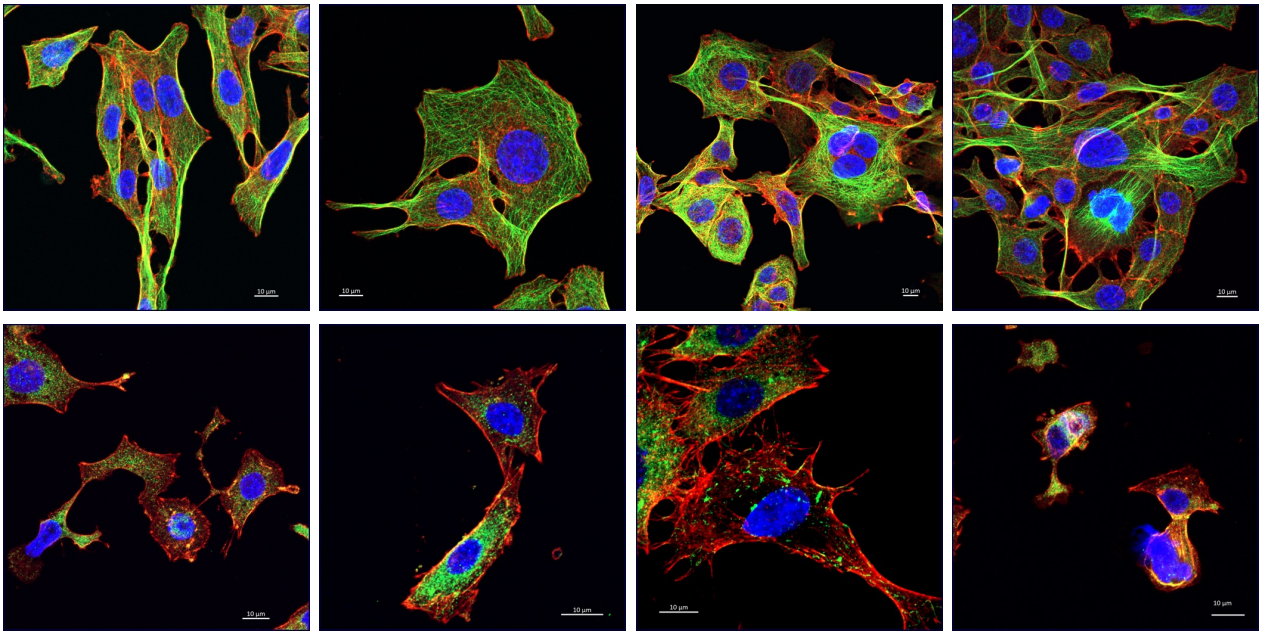

Supplementary Figure 9: Confocal images of Renca with and without treatment of LT-025 displaying tubulin disruption. The images showed disruption of the tubulin (green) crosslinking by DM1, a known microtubule inhibitor.

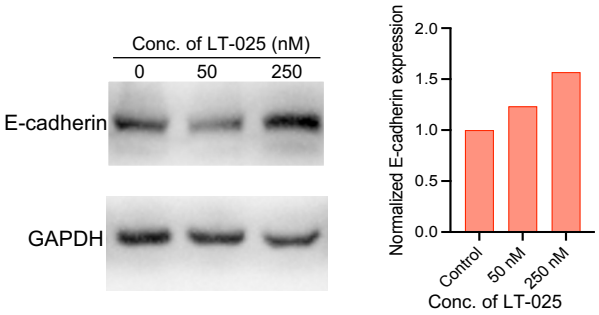

Supplementary Figure 10: Change in E-cadherin amount in Renca cells after treatment with LT-025. The western blot data (left) and its quantification with respect to the GAPDH intensity (right) show an increase in E-cadherin. This signifies a reduction in epithelial-mesenchymal transition (EMT) and lower metastatic potential.

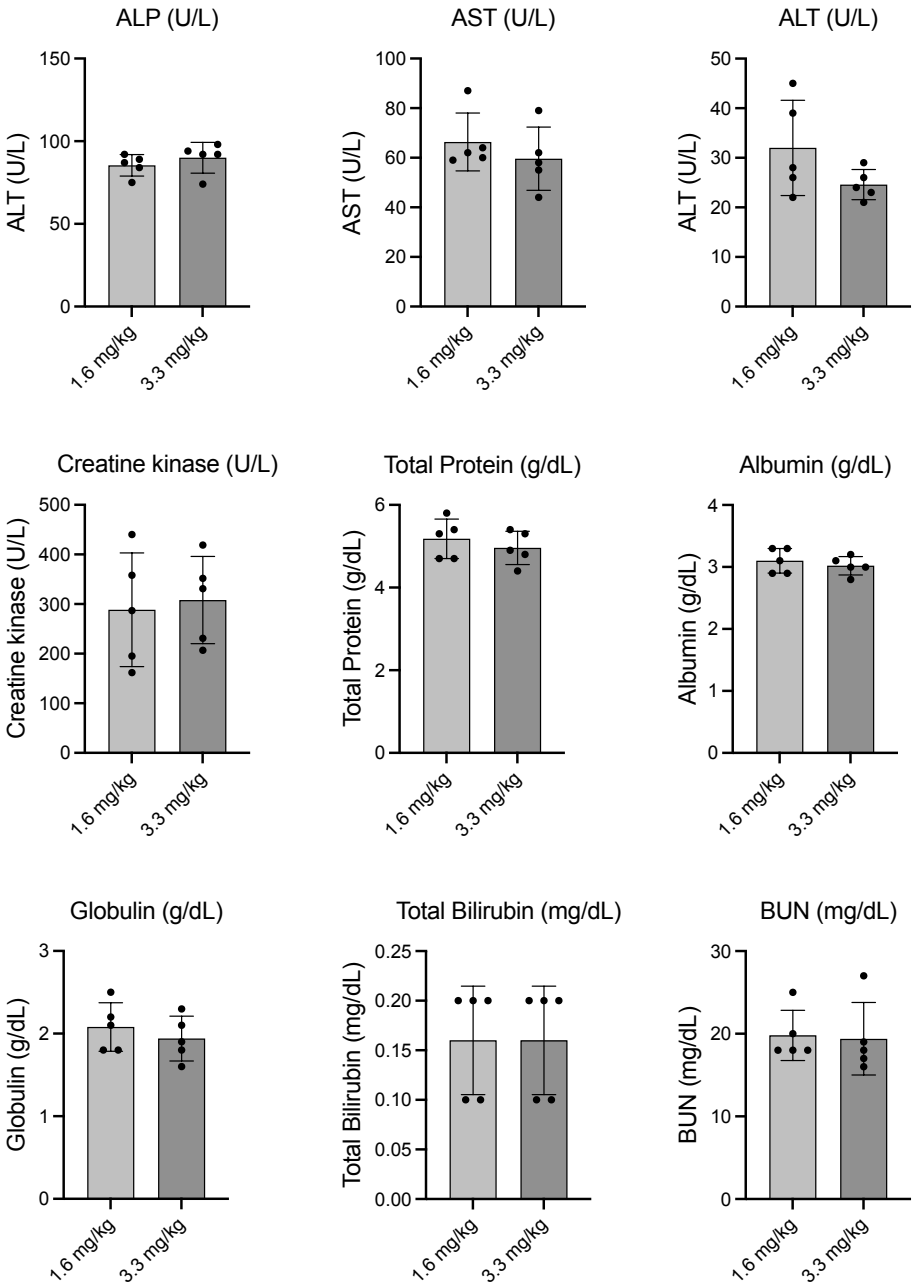

Supplementary Figure 11: Blood biochemistry analysis for the critical enzymes and blood components to evaluate any treatment-related toxicity in the dose escalation study of LT-025 in balb/c mice. Data shows no abnormal level, indicating safe treatment of LT-025.